Title

THE APPLICATION OF SURFACE PHYSICS TECHNIQUES TO THE STUDY OF ELECTROCHEMICAL SYSTEMS

Authors

Ross, P.N.
Wagner, F.T.

Publication Date

1983-07-01

Lawrence Berkeley Laboratory
UNIVERSITY OF CALIFORNIA

Materials & Molecular Research Division

To be presented at the International Society of Electrochemistry (ISE) in Erlangen, W. Germany, Spetember 18-23, 1983; and to be published in Advances in Electrochemistry and Electrochemical Engineering, Vol. III

THE APPLICATION OF SURFACE PHYSICS TECHNIQUES TO THE STUDY OF ELECTROCHEMICAL SYSTEMS

P.N Ross and F.T. Wagner

July 1983

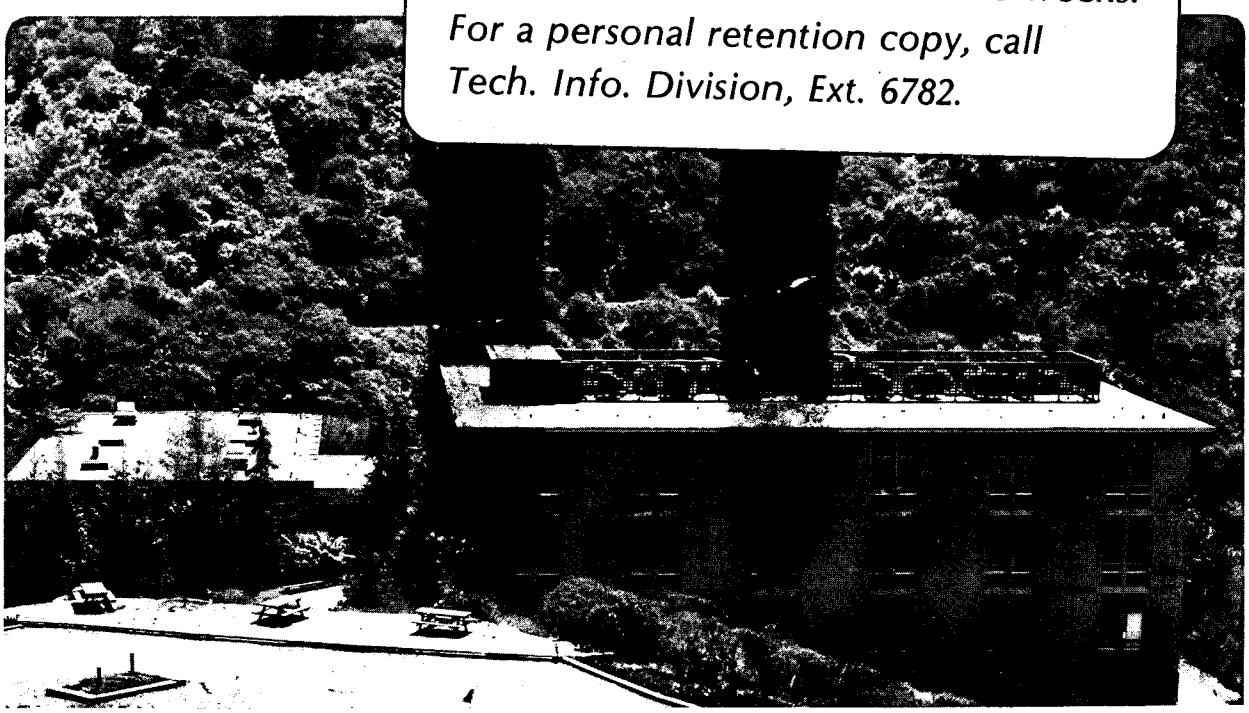

Prepared for the U.S. Department of Energy under Contract DE-AC03-76SF00098

DISCLAIMER

LBL-16235

THE APPLICATION OF SURFACE PHYSICS TECHNIQUES TO THE STUDY OF ELECTROCHEMICAL SYSTEMS

Philip N. Ross and Frederick T. Wagner

Lawrence Berkeley Laboratory
University of California
Berkeley, California 94720

July 1983

This work was supported by the Assistant Secretary for Conservation and Renewable Energy, Office of Advanced Conservation Technology, Division of Electrochemical Systems Resources of the U.S. Department of Energy under Contract No. DE-AC03-76SF00098.

Table of Contents

1. Introduction

The extraordinary growth within the last decade in the number of analytical techniques that can be applied to the study of the vacuum-solid interface has led many electrochemists to consider the application of some of these techniques to the study of the solid-liquid (electrolyte) interface. Many of these ultra-high vacuum (UHV) techniques use electron emission or electron scattering to probe the surface, and thus cannot be used directly, that is in situ. This is certainly the case with the now well-developed techniques of electron spectroscopy, e.g. Auger electron spectroscopy (AES), x-ray and UV photoemission spectroscopy (XPS and UPS), and electron diffraction, e.g. low energy electron diffraction (LEED) and reflection high energy electron diffraction (RHEED). There are also a number of surface spectroscopies, less well-known to the vacuum physicist, that can and have been used for in situ study of the solid-liquid interface, e.g. photon probes like ellipsometry and reflectance [1,2] and with the development of synchrotron radiation facilities in situ studies employing higher energy photons as probes will be come more prevalent [3]. In this article we shall review the use of familiar UHV surface spectroscopies applied ex situ to electrodes emersed from the electrolyte for the purpose of determining the atomic structure, composition, and chemical state of the electrode surface. It is apparent that if the electrochemist wants to determine the structure, composition, and chemical state of the

electrode surface in the electrolyte from this experiment, whether he can do so depends critically on what happens to the surface in both the emersion process and the process of transferring the surface to a vacuum system. Ideally, one wants to emerse the electrode from the electrolyte with the lowest possible coverage by residual electrolyte, i.e. only electrostatically bound ions and their hydration spheres, and also not have the surface react with the ionic layer when contact with the bulk electrolyte is broken, i.e. self-discharge. When the emersed surface is then exposed to vacuum for a sustained period, the ionic layer may or may not sublime from the surface depending on the adsorption energy, and characteristic probes of the surface will be affected by the presence of ionic species that remain on the evacuated surface (electrolyte residues). For the purposes of analysis of the solid side of the interface, residual ionic species complicate the interpretation of photon or electron scattering events at the surface and could easily render the experiment useless for the intended purpose. It is, therefore, easy to see that meaningful results from ex situ surface analysis can only be obtained with electrode -electrolyte combinations in which the emersion/evacuation processes are suitable for such analysis. Thus, detailed studies of the emersion and evacuation process must be an integral part of the ex situ study of each electrode/electrolyte combination.

There are, however, ex situ methods of surface analysis that are relatively insensitive to the presence of residual electrolyte on the surface and these methods can be applied to the analysis of emersed electrodes in a fairly general way. This is actually more fortuitous than it appears as one is not always interested in the chemistry of just the outermost surface layer, but in several atomic layers below the outer surface, as in anodic/passive layers on metals. X-ray photoemission and Auger electron spectroscopy (XPS and AES) are "near surface" spectroscopies, where the kinetic energy of the characteristic electrons are typically 100-1400 eV and the mean escape depths are 5-25 Å (2-10 atomic layers). Such spectroscopies could "see through" electrolyte residue (the non-volatile solute) if it were thin enough, but the fact that the spectra represent integration from several atomic layers also complicates the physical interpretation. XPS and AES have been used to study a variety of films [4 - 11], where in many instances the emersed electrode is rinsed with water and/or exposed to air. These types of "near surface" analyses do not require special apparatus, and the electrochemist can even have the surface analysis done by a colleague with a suitable UHV system. Air exposure and rinsing can drastically alter the properties of a surface due to reaction with air, to pH change and/or to self-discharge, or to contamination and are not generally valid procedures. For certain surfaces, such as passive films, these types of surface analyses can be informative, but they are not within the thrust of this chapter.

The principle thrust of this chapter is to discuss the experimental methods that have evolved out of several years of effort at different laboratories to study emersed electrodes by UHV techniques that probe the "outer" surface. We shall further focus the discussion to the problem of electrode surface structure determination by electron diffraction (LEED or RHEED), while giving examples of other types of studies that can be done with such apparatus. Low energy (<200 eV) electron scattering events, as in LEED, are very surface sensitive interactions, and only the first two atomic layers contribute to the electron scattering. It is imperative, therefore, that the emersion/evacuation process leave as little electrolyte residue as possible (ideally, none at all) and that the evacuation/transfer process not alter the surface due to reaction with residual gases in the vacuum/transfer system. The great need to minimize the undesirable effects in the emersion/evacuation and evacuation/transfer processes creates the mechanical complexity, and significant capital expense, of the apparatus for LEED studies.

2. Apparatus for UHV Analysis of Emersed Electrodes

There are several UHV systems worldwide that have been especially adapted or constructed for the study of emersed electrodes, and it is not possible to review them all here. We shall describe in some detail the system used in our laboratory, which is very similar, at least

conceptually, to systems in two other U.S. laboratories [12,13] The overall system is shown photographically in Figure 1. There are three principal subsystems, the UHV surface analytical chamber (labelled A in photograph), the transfer chamber (labelled B) and the electrochemical cell (on the end of the manipulator C_2). The UHV chamber has the LEED optics, a cylindrical mirror electron energy analyzer for electron spectroscopy, a quadrupole mass spectrometer, and an ion bombardment gun. The crystal under study is on a crystal mount that can be held either by the long-stroke magnetically coupled manipulator (labelled C_1) or by the offset manipulator in the UHV chamber. The crystal mount is held on manipulator C_1 for electrochemical experiments in a cell with a thin-layer type geometry. A detail of the electrochemical cell is shown in Figure 2. The single crystal is mounted on a Ta cup by a Au vacuum braze on the backside; the Ta cup is held in a stainless steel frame with a male bayonet that mates with a chlorofluoroethylene co-polymer (Kel-F) bayonet type holder on the end of manipulator C_1. The working crystal is therefore electrically isolated from the manipulator. The three-electrode cell consists of a ring counter electrode and disc reference electrode in a conventional ring-disc type of geometry; the counter electrode materials we have used are Pt, Au and vitreous carbon. The reference electrode material is usually Pd, which is charged with hydrogen to form an α-PdH reference, but can be a pure metal to form a Me/Me^{Z+} reference, e.g. Zn, Ag, Cu, etc.

The ring-disc is mounted in a PTFE block that is held in a Ta frame attached to the end of manipulator C_2. Electrolyte is introduced from an external reservoir (D in Fig. 1) via a PTFE capillary tube (d in Fig. 2) and forms a drop (ca. 100 μl) on the counter-reference ring-disc. When the working single crystal electrode is in place, a thin-layer cell is formed with electrolyte sandwiched between the crystal and the ring-disc. Electrical contact with the single crystal working electrode is made via a Pt spring-clip on the Ta cell-frame. The entire transfer chamber and cell are bakeable to 150 C with independent pumping of the chamber by a liquid nitrogen trapped turbomolecular pump. The electrochemical work station can be isolated from the UHV chamber by a gate valve (E). The baseline pressure in the transfer chamber after bakeout is ca. 5×10^{-9} torr, while in the UHV chamber it is 2×10^{-10} torr. Residual gas analysis by quadrupole mass spectrometer indicated the difference in pressure is due primarily to the higher partial pressure of H_2O, which probably arises from the lower bakeout temperature. However, the electrochemistry is not, and cannot, be done in a vacuum ambient (with aqueous electrolyte or with most non-aqueous solvent), so that the baseline pressure in these chambers is not the important criterion for system cleanliness. At the very least, the electrochemistry is done in a residual atmosphere of the solvent vapor at its room temperature vapor pressure, which for water is 23 torr. This would not seem, to the electrochemist, to pose any particular problem, since

no source of additional impurities (in addition to those present in the electrolyte) might be expected from the solvent vapor which is in equilibrium with the electrolyte. To a vacuum scientist, the problems are immediately apparent. Ultra-high vacuum is achieved by having the pumping speed far exceed the outgassing rate of all surfaces in the system, but there are very few UHV systems in which clean vacuum is maintained when the pumps are shut-off. This "wall-effect" is exascerbated by the introduction of any background gas to relatively high pressure (a few torr), which has a "knock-off" effect on contaminant molecules that had been gettered by the stainless steel walls of the vacuum chamber during bakeout. We have made a reasonably thorough study of the possibility of doing aqueous electrochemistry in a vacuum, maintained by continuous pumping and electrolyte feed, or in the absence of an invert backfill gas. Both these methods would minimize the "wall-effect," but we have concluded they are not practical methods, and even when used, did not appear to give better results than with the use of an inert backfill gas. The use of a backfill gas reduces the rate of evaporation of water (or solvent) and enables the experimenter to force electrolyte out of the cell, thus emersing the electrode in a well- controlled manner. The net result is that it is extremely difficult to maintain very low partial pressures (e.g. $<10^{-8}$ torr) of contaminants at the high total pressure (e.g. 20-800 torr) in the

electrochemical work station. The inert backfill gas must be incredibly pure, e.g. less than 0.1 ppb (!) in harmful impurities, and the walls of the chamber must be passivated to avoid "knock-off" contamination. These are requirements that are even more demanding than UHV practice and requires special procedures. In our system, commercial ultra-pure argon is used as the backfill gas, and it is further purified by passage through Ti sponge maintained at 900 C, cooled back to near ambient temperature by heat exchange from the stainless steel tubing line connecting the sponge capsule to the work station. The inside walls of the stainless steel were given an electropolishing treatment in addition to the usual surface finishing the commercial vendor applies to the components.

It is, however, clear that in spite of these extensive refinements of normal UHV practice and great care in the conduct of the experiment, some contamination of some surfaces does occur, either before a clean UHV-prepared surface can be examined electrochemically, or before an emersed electrode can be studied in the UHV chamber. Evidence of surface contamination is obtained by AES analysis in successive stages: i.) a clean, ordered, UHV-prepared surface is exposed to the backfill gas at near ambient pressure for several minutes, the gas rapidly turbopumped out to fairly high vacuum (ca. 10^{-8} torr), and the surface analyzed in the UHV chamber by AES; ii.) repeat of i.) with electrolyte (or solvent) vapor

added to the backfill gas at its equilibrium pressure, then rapid pump-out and analysis; iii.) contact with electrolyte with potentiostatic control in the thin-layer cell, emersion under potentiostatic control, pump-out and analysis. The resulting surface analysis by AES is shown in Fig. 3 for a Pt(100) crystal. The backfilling with purified argon, and pump-out, still leaves the surface relatively clean, as the C/Pt ratio indicated by spectrum 3b is 0.1 carbon atom per surface Pt [14]. However, exposure to electrolyte (0.3 M HF solution) vapor increased the C/Pt substantially, which we attributed to the "wall-effect" described above; contact with liquid electrolyte while potentiostatted at 0.8V RHE*, emersion, and pump-out did not increase the C/Pt ratio further. The contact with electrolyte also gave rise to trace levels ($<10^{13}$ atoms$\cdot$cm^{-2}) of sulfur and chlorine. The Pt(100) crystal surface at the instant of contact with electrolyte is clearly not perfectly clean, but has a carbonaceous contaminant of unknown chemical identity. This level of impurity is sufficient to affect the electrochemistry, as we have discussed before [15], but it does not have a deleterious effect on the LEED analysis of the surface, which will be reviewed in a subsequent section. The reasons that this contamination does not seriously affect LEED are that this concentration is sufficiently low so as not to greatly attenuate the diffracted beams and that the contaminant is disordered. The contamination problem is metal specific, as expected, since it represents an adsorptive interaction between the clean metal and gaseous molecules. Au single crystal surfaces show virtually no contamination in experiments like that in Fig. 3, and it is clear that electrochemistry on clean Au surfaces, prepared and characterized in UHV, is possible in this apparatus. Cu single

*All potentials in this chapter are referenced to the reversible hydrogen electrode in the same electrolyte (RHE).

crystals pick up more chlorine and less carbon than Pt crystals do with transfer, but use of the highly purified argon reduced the Cl surface concentration to an acceptable level. UHV studies [16,17] of the interaction of H_2O with Ni and Pt surfaces indicated that Ni surfaces prepared in UHV would exhibit a very different kind of behavior when subject to the sequence in Fig. 3. Clean metallic Ni is highly reactive towards water vapor and exposure to ca. 20 torr H_2O vapor at room temperature would result in dissociation and coverage of the Ni surface by O and OH species [16]. The conclusions from experiments like that shown in Fig. 3 is that some clean UHV- prepared metallic surfaces will react with either the electrolyte vapor or with impurity residual gases before potentiostatic contact can be made, but that additional contamination upon emersion and evacuation does not occur. Some noble metals like Au can be studied electrochemically directly from the UHV-prepared state and can be emersed from electrolyte for UHV analysis without significant contamination.

It is a difficult matter to determine whether the contamination problems with UHV- prepared Pt surfaces we have described here for our apparatus occurs in the apparatus of others [12,13], or whether another type of system or design would eliminate the problem altogether. There appears to be considerable controversy on this point, and it does not appear worthwhile to propagate it further here. It seems likely that improvements in the design of apparatus of the type described here will continue in our laboratory and elsewhere and that ultimately, perfectly clean Pt surfaces can be studied.

3. Emersion of Metal Electrodes

Understanding the emersion process is, as we have said, absolutely critical for the correct interpretation of ex situ spectroscopy, yet relatively few studies of this process have appeared in the literature. The most extensive, directly applicable work has come from the laboratories of Wilford Hansen, Utah State University, and Dieter Kolb of the Fritz-Haber Institute. They have used electro-reflectance [18], conductance [19], work function [20] and XPS [21] methods to study what is left on the surface of an electrode after the bulk electrolyte is removed. Earlier studies of electrolyte films on partially submersed electrodes [22-26] are not directly applicable to this question, since most of these refer to stationary (equilibrium) films and the emersion process is dynamic. However, Muller and co-workers [27] have made optical measurements of electrolyte films draining from vertical electrodes that are relevant to the emersed electrode problem. Using interferometry, Muller measured the electrolyte film thickness as a function of distance above the meniscus and the time increment after lowering the liquid level. For time intervals less than 60 mins., it was found that the results for a Ni surface in 3.4 N KOH, reproduced in Fig. 4, followed the relation for drainage of a Newtonian liquid from a vertical surface under gravitational and viscous forces,

$$y = \left(\frac{\mu}{\rho g}\right)^{1/2} \left(\frac{z}{t}\right)^{1/2}$$

where y is the film thickness, z the height of the film, μ the viscosity, ρ the density and g the gravitation constant. Stationary film geometry is not reached until after a period of some 10 hrs. The short time (5 min.) film thickness, which is closer to the time used for emersing electrodes in our work, is of the order of 3 μm, while the stationary film is ca.

0.5 μm. The nature of the interfacial forces that balance the hydrostatic pressure and lead to a stationary film are still not understood, as these films exist in the absence of any externally applied gradients of temperature or concentration. It is clear, however, that the film thickness during the emersion of the Ni electrode in Muller's experiments is controlled by viscous forces.

Much thinner electrolyte films on emersed electrodes are reported in the works of Hansen and Kolb. Hansen and co-workers [21] used quantitative XPS to determine the number of electrolyte ions that remained on the electrode surface after emersion and evacuation, from which the film thickness was deduced. Kolb and co-workers [20] have used work-function measurements and electro-reflectance to show qualitatively that some electrolyte is on the emersed surface, but the published work cited does not report a film thickness. In a joint paper [18], Hansen and Kolb reported that the XPS, ellipsometric, and electroreflectance determinations of film thickness were in agreement that the thickness of the water layer after emersion is of the order of 10 Å. They claim this is a general result, and do not restrict the conclusion to any particular class of electrode materials. However, most of the thickness determinations reported were obtained with tin oxide and indium oxide electrodes, with gold, silver and copper being mentioned as yielding the same type of emersion film. No physical explanation of these very thin films was presented, nor was there any reference to the earlier studies by Muller reporting much thicker films. The viscous

films observed by Muller are to be expected if the electrolyte has a wetting contact angle with the solid surface. Hansen and Kolb did not report contact angles, but they use terms like "hydrophobic behavior" and "hydrophobic state" which imply a hydrophobic non-wetting contact angle. It seems unlikely that hydrophobic contact angles are the general rule in solid electrode - aqueous electrolyte systems, and that it is more likely that Hansen and Kolb happened to have studied solids that exhibit hydrophobicity. Another possibility is that the electrode surfaces used were not clean, but were contaminated by hydrophobic adsorbates. Some indication of this possibility is seen in the work of Rath and Kolb [20], in which it was observed that "potential excursions into the oxide formation region with the gold disc had eventually caused the surface to become hydrophilic." They attributed this potential cycling effect to the creation of surface roughness, whereas anodic cleaning of the surface is also a possible explanation. There seems to be so much contradiction and uncertainty in the extant work on emersed film thickness that no prediction can be made at this time as to what thicknesses are to be expected in general.

Our own experiments on thickness of electrolyte films on emersed electrodes have not yet been published, although one brief communication is in press [28]. The electrode materials that we have studied with regards to electrolyte film thickness are Pt(100) in 0.3 M HF, Cu(111) in 10 mM HF, and Ni polycrystal in 1.5 and 15 mM $NaHCO_3$-Na_2CO_3. In all cases we observed

hydrophilic contact angles between the electrolyte and the UHV prepared clean metal surface. Auger electron spectroscopy of the residual concentration of Na^+ on the surface after emersion and evacuation was used to determine the film thickness. Quantitation of the Na^+ signal was achieved using spectra for reference compounds [29] and Lambert's Law of attenuation to derive an ionic sensitivity factor. As expected from the observed hydrophilic contact angles, we observed viscous films drawn during emersion, whose thicknesses were of the order of 1 μm for all three metals [28]. Our observations appear to be in agreement with the results of Muller for Ni in alkaline electrolyte. We have not, howeever, studied the particular electrode materials used by Hansen and Kolb, e.g. tin oxide, indium oxide, or gold, so it is not clear that there is a true disparity in observation. The existance of ca. 1 μm films on these metal electrode surfaces puts an upper limit on the usable concentration of non-volatile solute that can be used in electrolytes with ex situ surface analysis. A 0.4 μm film 5 mM in Na^+ results in a surface concentration of 1.1×10^{14} ions$\cdot$cm^{-2} equivalent to about one-tenth the surface concentration of most metals. We have obtained satisfactory LEED patterns from Cu(111) crystals that had ca. 10^{14} Na^+ ions$\cdot$cm^{-2} on the surface, but significantly higher concentrations would cause unacceptable diffuse backgrounds. Higher atomic number cations like K^+ or Cs^+, or anions like Cl^- or Br^-, which have stronger electron scattering power than Na^+, should be kept to surface concentrations below 10^{14} ions$\cdot$cm^2, which means using solute concentrations of ca. 1 mM.

It is easily seen, therefore, that even in the case of hydrophilic electrodes, and the drawing of relatively thick viscous films on emersion, it is still possible to use ex situ electron spectroscopy to study specific adsorption of ions since the effects of specifically adsorbed ions are apparent even at very low (e.g. 10μM) concentration and to use ex situ LEED to determine the atomic structure of the electrode surface. The distinction between hydrophilic and hydrophobic behavior of electrodes is not as restrictive as it might at first appear and in fact really only distinguishes two levels of usable electrolyte concentration, <1 mM and 10 mM-1M, respectively.

4. Selected Results Using Directly Coupled Systems

4.1 Adsorbed States on Emersed Electrodes Studied by Electron Spectroscopy and Thermal Desorption

It has already been demonstrated in the work of Hansen, et al. [21] that coverages of specifically adsorbed ions can be measured using electron spectroscopy with emersed electrodes. The particular system they studied, Br^- on Au, was a system which could be emersed and examined even with air exposure, due to the high adsorption energy of the Br^- ion and the weak interaction between Au and oxygen (or other neutral molecules that would be present in an air transfer). Electrode surfaces more reactive than

Au, or electroactive species less strongly adsorbed than Br^-, are likely to require the type of apparatus we have described here for coverage measurement. An example of this can be seen in work from our laboratory with Pt surfaces and the formation of underpotential states of oxygen [30]. Figure 5 summarizes the determination of the O/Pt ratio for a Pt(100) emersed electrode as a function of emersion potential using a combination of Auger electron spectroscopy and thermal desorption mass spectroscopy (TDS). The details of this experiments will be reported elsewhere [31]. There is a threshold potential below which no oxygen species are observed by either AES or TDS, and above which there is a nearly linear increase in coverage with potential. This threshold potential is ca. 1.2 V vs. RHE, but it is well-known that oxygenated species form on both polycrystalline Pt and Pt(100) at ca. 0.8 V [32]. This is shown dramatically by Fig. 6, which compares the O/Pt ratio determined by coulometry with that observed in vacuum by TDS. At ca. 1.4 V and higher the coulometry and TDS method are in reasonable agreement, but between 0.8 and 1.2 V the vacuum technique did not show any of the oxygen that was on the immersed surface. We attribute the "missing" oxygen to a combination of self-discharge and reaction with gas-phase reducing molecules during emersion/evacuation. The self-discharge of the adsorbed layer would seem to be a direct consequence of the reversibility of surface reaction

in the potential region of 0.8-0.9 V [33]. Above ca. 0.9 V, the oxygenated layer undergoes a transition, possibly involving place- exchange [34], which results in the oxygen species becoming kinetically irreversible, and thus, it is not discharged upon the loss of applied potential at emersion. In addition to losing the reversible oxygen species by self-discharge, some of the irreversible oxygen is also lost, probably by a "clean-off" reaction with carbon monoxide or hydrogen residual gases during evacuation and transfer. These results already show that only the irreversible and unreactive oxygenated Pt surface created at anodizing potentials above 1.2 V can be studied ex situ. We suggest that a similar circumstance may apply to other metal electrode systems of interest, i.e. only the passive metal oxide surface can be observed in electron spectroscopy of the emersed electrode.

There has been extensive use of XPS and AES to the study of anodic films on metals, and as we have pointed out in the experimental section, these studies do not necessarily require directly coupled UHV-electrochemistry instrumentation. We shall not, therefore, review that literature here, and the interested reader is referred elsewhere [4,11]. A lingering area of controversy in the literature of the passive film on iron is related to the nature of protons in the structure, and the extent to which the passive film becomes dehydrated during prolonged evacuation of emersed electrodes at room temperature [35]. The use of TDS to study the

dehydration behavior of the layer would help resolve problems in the interpretation of XPS and AES spectra. TDS studies are not easily done in "commercial" ESCA instruments, as such instruments usually do not have the requisite sample heating and mass spectrometer geometries, and it may be necessary to cool the electrode to below room temperature upon emersion to distinguish bulk water from water in the film. Thus, a directly coupled instrument appears necessary for this experiment. While we have not studied the dehydration of the surface of iron, we have studied the thermal decomposition of the anodic (passive) film on emersed Pt(100) electrodes by TDS [31]. For anodic films grown at potentials above ca. 1.4 V, water was observed in the TDS spectrum, as shown in Fig. 7 for an emersion potential of 1.8 V. Dehydration of the anodic film was observed at the surprisingly high temperature of 375 K. It is not possible, on the basis of this data above, to distinguish water produced by dehydration of an oxide hydrate

$$PtO_x \cdot y\ H_2O \rightarrow PtO_x + y\ H_2O$$

from water produced by disproportionation of hydroxide

$$Pt(OH)_{2n} \rightarrow PtO_n + nH_2O.$$

However, simultaneous measurement of the Pt:O:H_2O stoichiometries by TDS and XPS or UPS chemical shifts should result in an unambiguous determination of the chemical state of hydrogen in the anodic film. Similar kinds of experiments on passive films of iron should be equally informative. The dehydration temperture of 400 K for the anodic films on Pt(100) are significantly higher than the disproportionation temperatures reported by Fisher and Gland [17] for UHV formed OH species on Pt(111) or by Stuve, et al.[48], for OH on Ag(110), 210 and 320 K, respectively. However, the UHV created OH state is at very low (tenths of a monolayer) coverage, whereas the electrochemically formed films probably involve place exchange and the formation of a surface phase oxide. It seems likely that the higher disproportionation temperature found for the anodic film represents a collective interaction in the surface phase oxide that leads to the greater thermal stability. The Pt work indicates that anodic films are not dehydrated during evacuation to the extent some have suggested [35,37], but more extensive work using TDS should help to resolve this important issue for other metals.

Previous XPS studies by Hammond and Winograd [38] clearly demonstrated that the underpotential state of metals on metals can be studied by ex situ methods. To date only noble adatoms on noble metal surfaces, such as Cu and Ag on Pt have been studied in this manner, and

it is unclear whether base metals can be studied as well. Kolb [1] has discussed the problem of self-discharge of underpotential metals, when potential control is lost upon emersion. This would appear to be particularly problematic with any ad-atom state below the RHE in acidic solution, which include many systems of technological interest, e.g. Zn, Cd, Sn, and Pb. In preliminary experiments in our laboratory we have observed that underpotential Zn on Cu(111) is discharged upon emersion and is left as a zinc oxide deposit on the surface after evacuation. Hagans [39] attempted to observe the structure and chemical state of underpotential Pb on Au single crystals by LEED/AES, but the results were inconclusive with some indications from AES that the Pb was discharged upon emersion. However, for those metals where self-discharge is not a problem, XPS and UPS hold great promise for determining the formal valence for the underpotential state and the nature of the adatom substrate bond.

4.2 Structure Determination for Emersed Electrode Surfaces Using LEED

The number of studies in which the structure of an emersed electrode surface was successfully determined by LEED are extremely limited, and all very recent. Hubbard and co-workers [40] have obtained LEED patterns for Ag and Cu electrodeposited on an iodine pre-treated Pt(111) surface. The iodine pre-treatment was done in the UHV chamber before immersion of the single crystal electrode into electrolyte. Chemisorbed iodine

apparently protects the Pt surface and Ag and Cu ad-atoms from reactions with residual gases during transfer [41]. The LEED and AES analysis indicated that Ag and Cu are deposited underneath the iodine forming a highly ordered I-Ag(Cu) - Pt three-layer structure. For Ag, three differently ordered structures were observed that were directly related to three sharply defined peaks in the cyclic voltammetry of the Ag deposition. This study is an elegant example of the use of LEED to determine surface structures that correspond to distinct electrochemically formed phases. The particular experimental approach used by the Hubbard group, requiring the use of a very strongly adsorbing ionic species like I^- to protect the surface, restricts the general applicability of the resulting structure determination, as the structure of the Ag and Cu ad-layers is probably strongly affected by the presence of I^-. Hopefully improvements in the experimental methodology will enable the structure of Ag and Cu ad-layer on Pt to be determined in the absence of strongly adsorbing anions, or with anions of greater general interest.

The research group of Professor Ernest Yeager, Case Western University, and these authors have been using LEED to study the structural transformations to the low index surfaces of Pt during potential cycling through anodic film formation/reduction. Only a few publications are available at this time that describe the work to date[15,42], and we shall review those here. Angerstein - Kozlowska, et al. [34] have

proposed that place exchange occurs during anodic film formation on Pt which causes Pt atoms to move out of their 3-D fcc lattice positions. During reduction of the anodic film, the Pt atoms may or may not return to their original lattice sites depending on the order in the oxide and the Pt atom mobility. It is easy to see that the place exchange process can lead to disordering of the low index surface. The work from Yeager's group and that from our own work on the transformation occurring on cycling have arrived at some points of agreement and some points of differing interpretation. Both groups are in agreement that transformations in the low index surfaces occur as a result of potential cycling through the "irreversible oxide" potential region of 1.4-1.5 V RHE, and that the oxide formed at these potentials is itself "amorphous," i.e. produces no LEED pattern. There is, however, disagreement between the groups on the details of the transformation process, at what potential it begins, and what the real-space surface structure is after potential cycling. In order to understand the differences in interpretation of the LEED patterns both groups have observed, it is useful to review the features of LEED theory relevant to the problem. The relevant LEED theory is that for the study of structural defects in surfaces as developed by Legally [43] and Henzler [44]. A summary of types of defects in the real-space structure and the corresponding reciprocal-space feature, i.e. the effect on the diffraction pattern, is given in Table 1. As a result of the pioneering work of Somorjai [45] and co-workers with high Miller index surfaces of Pt, the most familiar defect structures for Pt are the "ordered step" structures, which contain monatomically high steps along major crystallographic directions in an ascending staircase arrangement with one another.

These "ordered steps" produce easily recognized characteristic LEED patterns with alternately split and sharp spots with changing beam energy [46]. Ion-bombarded surfaces have been observed [47] to produce LEED patterns which are closely related to those for "ordered steps", but have alternately broad (or diffuse) and sharp spots with changing beam energy. This type of LEED patterns has a corresponding real-space structure which has been termed a "randomly stepped" surface [43,44]. The randomly stepped surface has steps which are both up and down, rather than all up (or down) as in the "ordered step" structure, and the steps extend along a crystallographic direction only a finite distance, rather than being essentially infinite in extent in the "ordered step" structure. The regions between steps, the terraces, have the low index order and the widths of these terraces are randomly distributed about a mean value. Henzler has shown that one can determine the mean terrace width from the angular broadening of the spots and the step height from the incident energies at which the diffracted beams are sharp. This is the type of diffraction pattern we have reported [15] for Pt(100) surfaces cycled to 1.58 V RHE. We also see this type of LEED pattern on Pt(100) crystals that have been argon ion-bombarded in the UHV system. We shall return to a further discussion of the LEED patterns for cycled surfaces after reviewing other types of defect structures.

While step-like imperfections either periodic or random, lead to distinctive spot size vs. beam energy behavior, other types of surface imperfections yield less dramatic effects on diffraction patterns which nonetheless can be analyzed in some detail, as done by Henzler and Legally. If the size of the ordered domains of the surface are smaller than the coherence length of the instrument (typically 100-300 Å), broadening of all

LEED beams occurs at all energies. Point defects such as random adatoms or random vacancies add a diffuse background to the LEED pattern of the substrate. Random strain at the surface preferentially broadens diffraction spots of higher order, leaving the (0 0) spot sharp. A mosaic of crystallites produces a LEED pattern that is a sum of patterns from each crystallite with the angular divergence between crystallites causing increased apparent broadening of all spots as the beam energy is increased. A partial overlayer may consist of domains which are commensurate with the substrate, but which are out of phase with one another. If these "anti-phase domains" are smaller than the instrumental electron coherence length, a LEED pattern containing both sharp and broadened (or split) spots may result. In this case, the relative widths of any two spots of different symmetry remain unchanged by a variation in the incident beam energy. This invariance allows ready distinction between LEED patterns due to anti-phase domains and those due to steps. Under some conditions generally involving chemical etching or thermal annealing, a given crystal face may facet into microfacets of more stable orientations. If the facets are larger than the coherence length of the instrument, two (or more) independent LEED patterns will be seen simultaneously. Each pattern will have its own (0 0) spot towards which the other spots will migrate as the beam energy is increased. Since all facets are part of the same 3-D crystal, spots due to the different faces will coalesce at beam energies corresponding to 3-D reciprocal lattice points to form a single sharp spot. If the beam energy is then increased, the spot splits, with the diffraction spot due to each facet orientation moving off towards the appropriate (0 0) beam. As the facet size drops below the instrumental coherence length, resolution of the split spots is lost and one obtains instead a

single spot broadened out towards the various (0 0) beams. At the limit of very small facet sizes, the LEED pattern would be indistinguishable from that for a randomly stepped surface. In this limit, however, the real-space surface would also be aptly described by either the facetted or the stepped surface model.

The Yeager group has reported that for Pt(111), (100) or (110) surfaces cycled to 1.4 V RHE no LEED patterns were observed at beam energies below 100 V. At higher beam energies on (111) and (100), weak diffraction spots characteristic of the (1x1) low index face were observed against a strong diffuse background [42]. They have interpreted these patterns as indicative of a totally disordered Pt overlayer on the ordered underlying substrate. As discussed above, strong diffuse background is characteristic of a disordered overlayer and/or random adatoms and vacancies. However, it is not certain that the disordered overlayer consists of Pt atoms, and our results suggest that the diffuse background is caused by a disordered overlayer of impurities. We also observed strong diffuse backgrounds on cycled Pt surfaces if the crystal was emersed from the electrolyte by straight separation of the thin-layer cell in Fig. 2, which was the emersion procedure used by Homa [42] in their thin-layer cell. This separation procedure, in our experience, leaves a very thick (ca. 1 mm) electrolyte layer on the surface, and that evaporation of this layer deposits non-volatile impurities on the surface in nearly monolayer amounts. These impurities are likely to be cationic, Ca^{2+}, Na^{+}, K^{+} etc. and need only be present at ca. 10^{-6} mol/ℓ to result in surface concentrations upon evacuation of a ca. 1 mm film of ca. 10^{14} ions/cm^2. Because of the low AES sensitivity of alkali metal cations [29],

such levels would be extremely hard to detect. These cations carry associated water which is not lost on evacuation, as shown by TDS, and the hydrated cations have very strong low energy electron scattering cross-sections, and can cause a strong diffuse background even at coverages as low as 10^{14} ions/cm^2. When we use the emersion procedure described in the previous section, which results in ca.1 μm electrolyte layer, three-orders of magnitude thinner than the straight separation procedure, we did not observe strong diffuse background. Instead, we observed the well-contrasted diffraction patterns that were reported in Ref. 15. Diffraction patterns analogous to those in Ref. [15] are shown in Figs. 8-11, as well as some new results shown in Fig. 14. Figure 8 shows the LEED pattern for a clean Pt(100) surface prepared in UHV. The complex pattern of multiple spots (the "5x20" reconstruction) is generally believed to result from the presence of a hexagonally closest packed surface layer on top of the square meshed substrate [49]. In the presence of small coverages of almost any adsorbate this reconstructed surface reverts back to the 1x1 termination of the bulk structure [50]. This transition entails a decrease of at most ~15% in the number of surface platinum atoms per unit area. In our apparatus the 5x20 reconstruction survives at least 15 minutes in the unpumped transfer chamber as long as no argon is admitted. However, after a backfill to atmospheric pressure followed by pumpdown, the surface transforms to the 1x1 structure as shown by the LEED pattern in Fig. with all of the 1x1 spots sharp at all energies. Figure 10 shows the LEED pattern for a UHV- prepared Pt(100) surface which was contacted with 0.3 M HF at 0.4 V RHE, swept ten times at 100 mV/s between 0.02 and 0.82 V RHE, and separated from the electrolyte while

potentiostated at 0.4 V. No significant differences between this LEED pattern and the one exposed merely to the Ar backfill (Fig. 9) are observed by LEED at any incident beam energy. Thus contact with the electrolyte and potentiodynamic cycling to the edge of the oxygen electrosorption region causes no discernable change in the structure of the surface. Figures 10-12 show the effects of extending the upper sweep limit to 1.58 V RHE on LEED patterns taken at different incident beam energies. At 176 eV the (11) spots are sharp while the (10) and (20) spots are broadened. At 134 eV the (10) and (20) spots are sharp while the (11) spots are broadened. At 114 eV the (11) spots are sharp, the (10) spots are broadened and the (20) spots are off the screen. The alternating pattern continues down to the lowest beam energy at which spots are visible, as shown by the LEED pattern in Fig. 13 for 60 eV, which has sharp (11) spots and diffuse (10) spots. In contrast to the observations reported by Yeager, et al. [42], we do see well-contrasted LEED patterns at beam energies below 100 eV.

Of all the defect types described in Table 1, only random steps can yield LEED patterns with the observed periodic variation in the angular width of diffraction spots as the incident beam energy is changed. The fact that every LEED beam is sharp at some energies indicates that most of the Pt atoms are still in 3-D fcc lattice positions. The LEED patterns in Figs. 10-13 indicate that limited potentiodynamic cycling into the "oxide" formation potential has shifted many atoms out of the ideal planar surface

but has left them in 3-D lattice sites. The energies at which sharp (10), (20), and (11) spots occur are all in good agreement with energies calculated for coherent scattering from adjacent (100) planes (see Ref. 15). No local minima in width are apparent between these 3-D Bragg energies as would occur if oligatomic (<5) step heights predominated. If a large proportion of multiatomic (≧5) step heights were present, the Lu and Legally [51] calculations indicate that the spot width would be almost constant except at beam energies very close to the 3-D Bragg conditions, where a sharp spot would be seen. Since the electrochemically cycled Pt(100) surfaces show a more gradual transition between minimum and maximum spot size, it would appear that multiatomic step heights are not present in great numbers.

The maximum LEED spot size from a randomly stepped surface is inversely related to the mean terrace width. For a geometric (random) distribution of terrace widths with monatomic step heights, the spot widths in Figs. 10-13 equate to a mean terrace width of ~5 atoms or 13 Å. Coulometric repulsions between steps lead one to expect a more correlated (less random) terrace width distribution. Henzler [52] obtained the best fit to beam profile data for etched semiconductor surfaces with an empirical distribution of terrace sizes somewhat more highly correlated than a random distribution. Assumption of this empirical distribution in the present experiment leads to a mean terrace width of ~7 atoms or 19 Å. The presence of multiatomic step heights would decrease the apparent mean terrace width corresponding to a given spot width. The most probable configuration of the 1.58 V cycled surface is a random up-and-down series of monatomic atomic steps

connected by (100)-(1x1) ordered terraces of 5-7 atoms. The step-site (dislocation) density for the Pt(100) surface cycled ten times to 1.58 V is therefore ca. $3x10^{14}$ sites cm^{-2} and the ordered (100) site density is ca. $12x10^{14}$ sites$\cdot cm^{-2}$, so about one site in four on this surface is associated with a step-site. A Pt(100) surface cycled only to 0.82 V has a structure with longer range order, with a dislocation density of only $5x10^{13}$ sites$\cdot cm^{-2}$ or less.

Recent work in our laboratory has shown the LEED analysis may be able to follow the place exchange process during anodic film formation. Examples of this are shown in Fig. 14. The LEED pattern at constant incident beam energy shows changes in the (10) and (20) spot profiles as a function of the anodic potential limit of the cycle. Note that the (10) and (20) spots for 1.08V cycles have sharp bright centers with "halos"; for 1.28V cycles the (10) and (20) spots have just the halos or rings; for 1.58V cycles the (10) spots are uniformly broadened while the (20) spots appear to have some internal structure. Variations in spot profile like these are indicative of real-space structural differences due to the increased anodic potential. The presence of sharp central peaks after ten cycles to 1.08 V suggests that fairly extensive, atomically flat regions (terraces), remain. Henzler's [52] calculations have shown that randomly stepped surfaces with moderately wide distributions of terrace widths can lead to spots with profiles similar to the "halos" seen after ten cycles to 1.28 V; the diameter of the intensity maximum in the halo indicate a mean terrace width of 23 Å. The flat-topped beam profiles seen after cycling to higher potentials are consistent with a further broadening of the terrace width distribution. The successive changes in spot profile observed after cycling to successively higher anodic limits suggest a progressive introduction of step

sites and a decrease in the size of terrace regions. At a given potential within the oxide region, increasing the number of cycles had an effect on the LEED pattern similar to that of cycling to successively higher potentials.

The production of steps is apparently due to the vertical displacement of Pt atoms (the place exchange) into a disordered surface phase during the anodic sweep. Subsequent reduction in the cathodic sweep returns most of the Pt atoms to 3-D lattice sites, but not exclusively to the 2-D lattice sites of the original low-index surface, i.e. the metal surface becomes vertically extended. Identification of the lowest potential at which LEED beam broadening occurs thus establishes the onset potential for place exchange. Determination of the number of cycles required to produce a given broadened beam profile at different potentials can provide a statistical determination of the fraction of all atoms displaced per cycle (i.e. the extent of place exchange) as a function of potential.

It is difficult to assemble a real space representation of imperfect surfaces, such as a ball-model, as the number of atoms required to reasonably represent the unit cell would be of the order of 2500. For many purposes, the statistical determination of terrace site density and the step-site density is sufficient and such determinations are relatively easily made as we have described here. An example of this is the use of LEED to determine the relation of the underpotential peaks for hydrogen to the surface structure of the Pt. Since the saturation coverage by hydrogen on a Pt(100) surface cycled to 1.5 V several times is ca. 15×10^{14} H atoms$\cdot$cm^{-2} [32], and the LEED analysis indicates the step-site density is ca. 3×10^{14} sites$\cdot$cm^{-2}, it is clear that most of the hydrogen in the

underpotential peaks is associated with the (100)-(1x1) ordered terraces on the surface and not the step-sites. There are changes in the voltammetry of Pt(100) that occur as a result of cycling the surface to 1.4-1.6V that Yeager, et al. [42] have attributed to the changes to the surface structure Since these changes are voltammetry features that disappear upon cycling, the features must be associated with the long-range order (>100 Å) in the surface, since short-range order (20 Å) is still preserved. Electrochemical processes that require long-range order are not well-known, and suggest collective interactions in the double-layer which could be extremely interesting. However, we have reported [15] that these features are not associated with long-range order in the surface but with impurities that are irreversibly oxidized during the cycling to 1.4-1.5 V. This conclusion was supported by experiments with UHV ion-bombarded surfaces of Pt(100) that had the same type of surface structure as the electrochemically cycled surface but still produced the anomalous voltammetry features [42] on the first cycles to anodic limits below 0.8 V. Even though complete physical models of imperfect surfaces can be difficult to derive, the statistical determinations of the surface structure by LEED as we have described is capable of establishing structure-property relations.

5. Concluding Summary

The use of electron spectroscopy (XPS,UPS) and low energy electron diffraction (LEED) to study the surface chemistry and surface structure of emersed electrodes in proving to be a valuable new tool for electrochemical research. These ex situ techniques are, however, fundamentally limited and cannot be universally applied to all electrode-electrolyte systems due to changes which may occur during electrode emersion. Insufficient attention had been paid to possible changes to the surface on emersion in many early ex situ studies. There appears to be considerable discrepancy in recent observations of the thickness of residual electrolyte films on emersed electrodes, and whether these films are 0.01 μm or 1.0 μm is an important factor in the interpretation of ex situ surface analyses. A better understanding of the emersion process and how it varies with different electrodes, electrolytes and emersion procedures will be necessary to determine the general applicability of ex situ surface analyses. In the last few years, improvements in the methodology of directly coupling electrochemical cells to UHV systems has enabled LEED determinations of the surface structure of emersed electrodes to be made with certain electrode-electrolyte systems. These recent observations presage an exciting new era in electrochemical science where specific electrode processes can be related to surface structures in a definitive way. Interestingly, two of the electrochemical systems which have been studied by LEED happen to represent two very different kinds of surface structures and two different kinds of LEED analysis were used. These studies reflect in a very positive way on the flexibility of LEED analysis of surface structure despite misgivings expressed about LEED in this regard [53]. In the recent studies by Hubbard and co-workers, the periodicity of the superstructure of underpotential Ag on iodine covered Pt(111) as observed directly

by LEED was combined with independent measurements of coverage (coulometry and Auger electron spectroscopy) to infer a real- space structure for the overlayer. This type of structure deduction has been widely used in the study of UHV created surfaces (usually adsorbed phases), but it is limited to surface structures which are nearly perfectly ordered. It is frequently the case in vacuum deposition that even in epitaxial growth of metal overlayers on like metals that the resulting structure is imperfect. For electrochemical processes like electrodeposition, especially multilayer deposition, there should be an analogous expectation that these surfaces may have an imperfect real- space structure that can only be described in a statistical way, e.g. the average dislocation site density, the dislocation site geometry, the ordered terrace dimension, etc. Nonetheless, the statistical determination of the order in the surface as the authors have done for an electrochemically modified Pt(100) surface will be a major step forward in the current state of knowledge of the atomic structure of electrode surfaces and of the transformations that occur during electrochemical processes. There are also some recent indications that thermal desorption spectroscopy (TDS), another workhorse tool for UHV surface studies, can be meaningfully applied ex situ to the study of electrochemically grown surface phases. Of particular immediate interest is the use of TDS to study the dehydration behavior of anodic (passive) films; together with XPS/UPS, TDS may provide unambiguous determination of the state of hydrogen (H atoms) in such films. There are numerous other UHV techniques in addition to XPS/UPS, LEED, and TDS being developed for the study of the vacuum/solid or gas/solid interface, e.g. ion-scattering spectroscopy, vibration spectroscopy from electron energy loss, and it

is expected that these techniques will also be applied to the study of electrochemical systems as the use of ex situ analysis matures as a scientific method.

Acknowledgments

The authors acknowledge support for the preparation of this chapter from the Assistant Secretary for Conservation and Renewable Energy, Office of Advanced Conservation Technology, Division of Electrochemical Systems Resources of the U.S. Department of Energy under Contract No. DE-AC03-76SF00098. The authors express appreciation to Professor Ernest Yeager for providing us with manuscripts prior to publication and for discussions on unpublished results from his group.

References

1.) D. M. Kolb, in Advances in Electrochemistry and Electrochemical Engineering, Vol. 11, H. Gerischer and C. Tobias eds., Wiley-Interscience, New York, 1973, pp. 125-272, and references therein.

2.) G. A. Bootsma, L. J. Hanekamp and O. L. J. Gyzeman, in Chemistry and Physics of Solid Surfaces IV, R. Vanselowe and R. Howe eds., Springer-Verlag, 1982, pp. 77-107, and references therein.

3.) Physics Today, 34, 40 (1981).

4.) K. Kim, N. Winograd, and R. Davis, J. ACS, 93, 6296 (1971); J. Hammond and N. Winograd, J. Electroanal. Chem., 78, 55 (1977).

5.) C. Sayers and N. Armstrong, Surf. Sci., 77, 301 (1978); N. Armstrong and R. Quinn, Surf. Sci., 67, 451 (1977).

6.) A. Roches, J. Soloman and W. Baun, Appl. Surf. Sci., 7, 83 (1981).

7.) C. Anderson, S. James, W. Kilroy, and R. Lee, Appl. Surf. Sci., 9, 388 (1981).

8.) G. Burstein and R. Newman, Appl. Surf. Sci., 4, 162 (1980); G. Burstein and T. Hoar, Corr. Sci., 18, 75 (1978).

9.) H. Mathieu, J. Mathieu, D. McClure, and D. Landolt, J. Vac. Sci. Tech., 14, 1023 (1977).

10.) P. Sherwood, Surf. Sci., 101, 619 (1980) and references therein.

11.) R. Koetz, H. Lewerenz, and S. Stucki, J. Electrochem. Soc., 130, 825 (1983).

12.) E. Yeager, A. Homa, B. Cahan, and D. Scherson, J. Vac. Sci. Technol., 20 628 (1982).

13.) R. Ishikawa and A. Hubbard, J. Electroanal. Chem., 69, 317 (1976); A. Hubbard, Accounts Chem. Res., 13, 177 (1980); A. Hubbard, J. Vac. Sci. Tech., 17 49 (1980).

14.) Based on the C/Pt AES calibration established by S. Davis, B. Gordon, M. Press and G. Somorjai, J. Vac. Sci. Technol., 19, 231 (1981).

15.) F. Wagner and P. N. Ross, J. Electroanal. Chem., in press.

16.) C. Brundle and A. Carley, Faraday Disc. Chem. Soc., 60, 51 (1975).

17.) A. Fisher and J. Gland, Surf. Sci., 94, 446 (1980).

18.) D. Kolb and W. Hansen, Surf. Sci., 79, 205 (1979).

19.) W. Hansen, C. Wang, T. Humpherys, J. Electroanal. Chem., 90, 137 (1978); W. Hansen, Surf. Sci., 101, 109 (1980).

20.) W. Hansen and D. Kolb, J. Electroanal. Chem., 100, 493 (1979); D. Rath and D. Kolb, Surf. Sci., 109, 641 (1981).

21.) W. Hansen, D. Kolb, D. Rath and R. Wille, J. Electroanal. Chem., 110, 369 (1980).

22.) F. Will, J. Electrochem. Soc., 110, 145 (1963).

23.) Y. Chizmadzhev and V. Markin, Sov. Electrochem., 2, 1245 (1966).

24.) V. Shepelin, Sov. Electrochem., 3, 896 (1967).

25.) R. Burshtein, M. Tarasevich, S. Chernyshyov, and V. Karesev, Sov. Electrochem., 3, 803 (1967).

26.) E. Lightfoot and V. Ludviksson, J. Electrochem. Soc., 1325 (1966).

27.) R. Muller, J. Electrochem. Soc., 113, 943 (1966); J. Turney, Lawrence Berkeley Laboratory Report LBL-171, 1971; M. Sand, Lawrence Berkeley Laboratory Report LBL-3589, 1975.

28.) F. Wagner and P. Ross, J. Electrochem. Soc., in press.

29.) Handbook of Auger Electron Spectra, Physical Electronics Industries, Eden Prairie, Minn., Second Edition, 1976.

30.) F. Wagner and P. Ross, ECS Proceedings Volume 83-1, The Electrochemical Society, 1983, Extended Abstract No. 802.

31.) F. Wagner and P. Ross, submitted to Surface Science, 1983.

32.) P. Ross, Surf. Sci., 102, 463 (1981).

33.) P. Stonehart, H. Kozlowska, and B. Conway, Proc. Roy. Soc., A310, 541 (1969).

34.) H. Angerstein-Kozlowska, B. Conway and W. Sharp, J. Electroanal. Chem., 43, 9 (1973).

35.) S. Tjong and E. Yeager, J. Electrochem. Soc., 128, 2251 (1981).

36.) G. Long, J. Kruger, D. Black, and M. Kuriyama, J. Electrochem. Soc., 130, 240 (1983).

37.) W. O'Grady, J. Electrochem. Soc., 127, 555 (1980).

38.) J. Hammond and M. Winograd, J. Electroanal. Chem., 80, 123 (1977); J. Electrochem. Soc., 124, 826 (1977).

39.) P. Hagans, Ph D Thesis, Case Western Reserve University, Cleveland, OH, 1979.

40.) J. Stickney, S. Rosaseo, D. Song, M. Soriaga and A. Hubbard, ECS Proceedings Vol. 83-1, The Electrochemical Society, 1983, Extended Abstract No. 700 and references therein.

41.) J. Katekarn, G. Garwood, J. Hershberger, and A. Hubbard, Surf. Sci., 121, 396 (1982).

42.) A. Homa, E. Yeager and B. Cahan, J. Electroanal. Chem. in press 1982; A. Homa, Ph D Thesis, Case Western Reserve University, Cleveland, OH, 1982.

43.) M. Legally in Chemistry and Physics of Solid Surfaces IV, R. Vanselow and R. Howe, eds., Springer-Verlag, 1982, pp. 281-311, and references therein.

44.) M. Henzler, Appl. Surf. Sci., 11/12, 450 (1982), and references therein.

45.) D. Blakely and G. Somorjai, Surf. Sci., 65, 419 (1977) and references therein.

46.) M. Henzler, Surf. Sci., 19, 159 (1970); 22, 12 (1970).

47.) D. Welkie and M. Legally, J. Vac. Sci. Technol., 16, 784 (1979); G. Schulze and M. Henzler, Surf. Sci., 73, 553 (1978).

48.) E. Stuve, R. Madix and B. Sexton, Surf. Sci., 111, 11 (1981).

49.) M. Van Hove, R. Koestner, P. Stair, J. Biberian, L. Kesmodel, I. Bartos and G. Somorjai, Surf. Sci., 103, 189 (1981).

50.) J. Gland and G. Somorjai, Advan. Colloid. Interface Sci., 5, 205 (1976).

51.) T. Lu and M. Legally, to be published in Surf. Sci.; also see T. Lu, S. Anderson, M. Legally and G. Wang, J. Vac. Sci., Technol, 17, 207 (1980).

52.) M. Henzler, Surf. Sci., 73, 240 (1978).

53.) D. Kolb and G. Zehmpfuhl, J. Electrochem. Soc., 127, 243 (1980).

Table 1. Correspondence Between Characteristic Imperfections in Surface Structure and LEED Pattern Features.

	DEFECT TYPE	DIFFRACTION EFFECTS
1)	disordered overlayer	diffuse background
2)	ordered overlayer, large domains	additional spots or change in intensity-energy profile (1x1 overlayer)
3)	random adatoms	diffuse background
4)	random vacancies	diffuse background
5)	small (<100 Å) domain size	all spots broadened at all beam energies
6)	random strain	broadening greater for diffraction beams of higher order
7)	mosaic structure	increased broadening of all spots with increasing beam energies
8)	antiphase domains	some spots sharp, others broad at all energies
9)	facetting	multiple (00) beams
10)	ordered steps	alternately split and sharp spots with changing beam energy
11)	random steps	alternately sharp and broadened spots with changing beam energy

Figure Captions

Fig. 1. Photograph of the directly coupled UHV-Electrochemistry apparatus at the Lawrence Berkeley Laboratory. A: surface analytical chamber; B: differentially pumped transfer chamber; C_1: transfer manipulator; C_2: electrochemical cell manipulator; D: PTFE external electrolyte reservoir with electrical feedthrus to cell; E: gate valve for isolation of transfer chamber from the turbo-molecular pump; F: wire electrode manipulator.

Fig. 2. Photographic detail of the electrochemical cell in position in the transfer chamber with a single crystal working electrode in place. a: Pt single crystal Au brazed to Ta block and mounted in 316 stainless steel bayonet holder; b: Pt ring counter electrode; c: Pd disc reference electrode; d: PTFE block mount for reference/counter ring-disc assembly.

Fig. 3. AES spectra of a Pt(100) single crystal at successive stages in the transfer from UHV to immersion and emersion.

Fig. 4. Electrolyte film thickness for vertically draining KOH from Ni as a function of time. From Ref. [27].

Fig. 5. Determination of the O/Pt ratio for the emersed Pt(100) electrode by ex situ analysis: (a) atomic ratio by TDS, (b) AES signal ratios as a function of potential.

Fig. 6. Comparison of O/Pt ration on Pt(100) determined by coulometry and by TDS ex situ of the emersed electrode as a function of potential.

Fig. 7. Thermal desorption spectra for a Pt(100) crystal emersed at 1.8 V (RHE) showing H_2O (M/e = 18) and O_2 (M/e = 32) emission from the surface. Heating rate ca. 10 $K \cdot sec^{-1}$.

Fig. 8. LEED pattern for clean, annealed Pt(100) surface in UHV. Beam energy 76 eV.

Fig. 9. LEED pattern for Pt(100) after exposure to electrolyte vapor and after immersion in electrolyte and cycling 10 times from .02 V to 0.82 V (RHE). Emersion potential 0.4 V. Cycling conditions: 100 $mV \cdot sec^{-1}$, 0.3 M HF.

Fig. 10. LEED pattern for Pt(100) after 10 cycles to 0.82 V compared to 10 cycles to 1.58 V. Emersed at 0.4 V. Incident beam 176 eV.

Fig. 11. LEED pattern comparison as in Fig. 10 at 134 eV.

Fig. 12. LEED pattern comparison as in Fig. 10 at 114 eV.

Fig. 13. LEED pattern for Pt(100) crystal cycled 10 times to 1.58 V at an incident beam energy of 60 eV. Cycling conditions as in Fig. 9.

Fig. 14. The effect of anodic potential limit on the LEED patterns for Pt(100) at an incident beam energy of 176 eV. Cycling conditions were 10 times from a cathodic limit of 0.02 V at 100 $mV \cdot sec^{-1}$ in 0.3 M HF. Emersion potential was 0.4 V in each case.

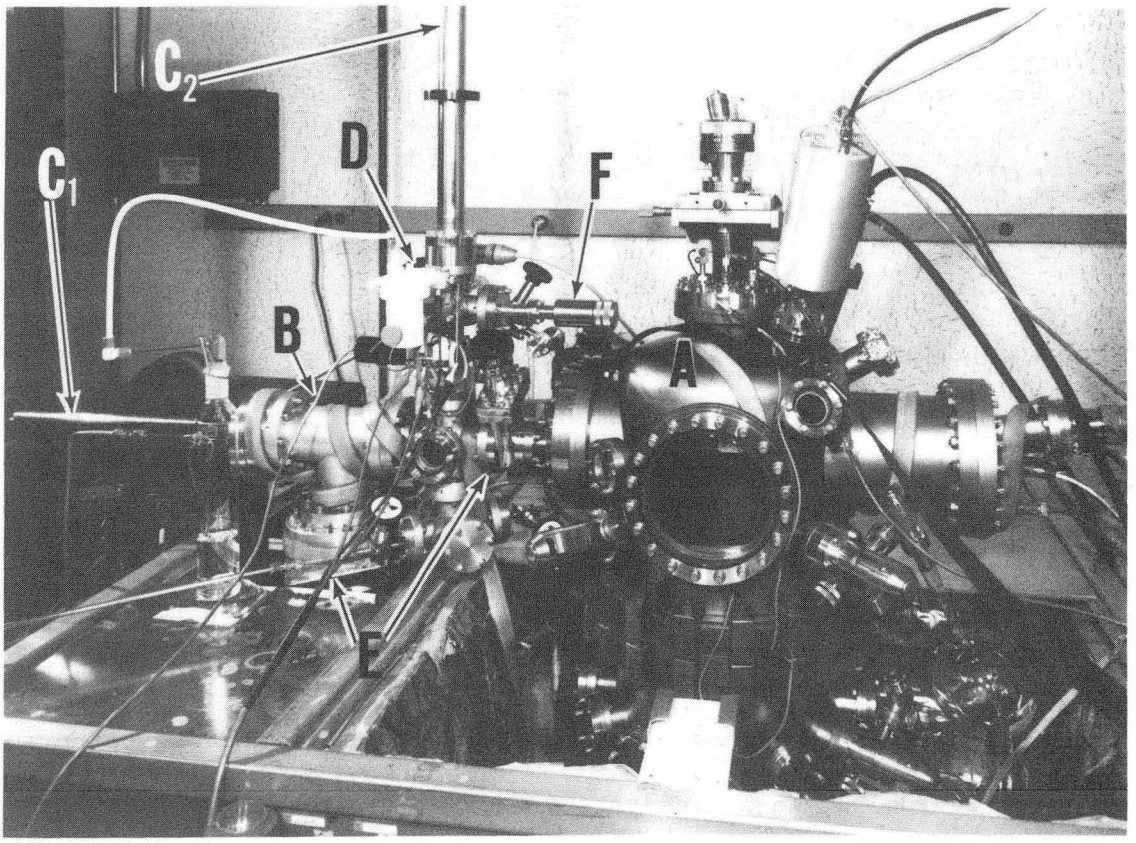

XBB 824-3085A

Fig. 1

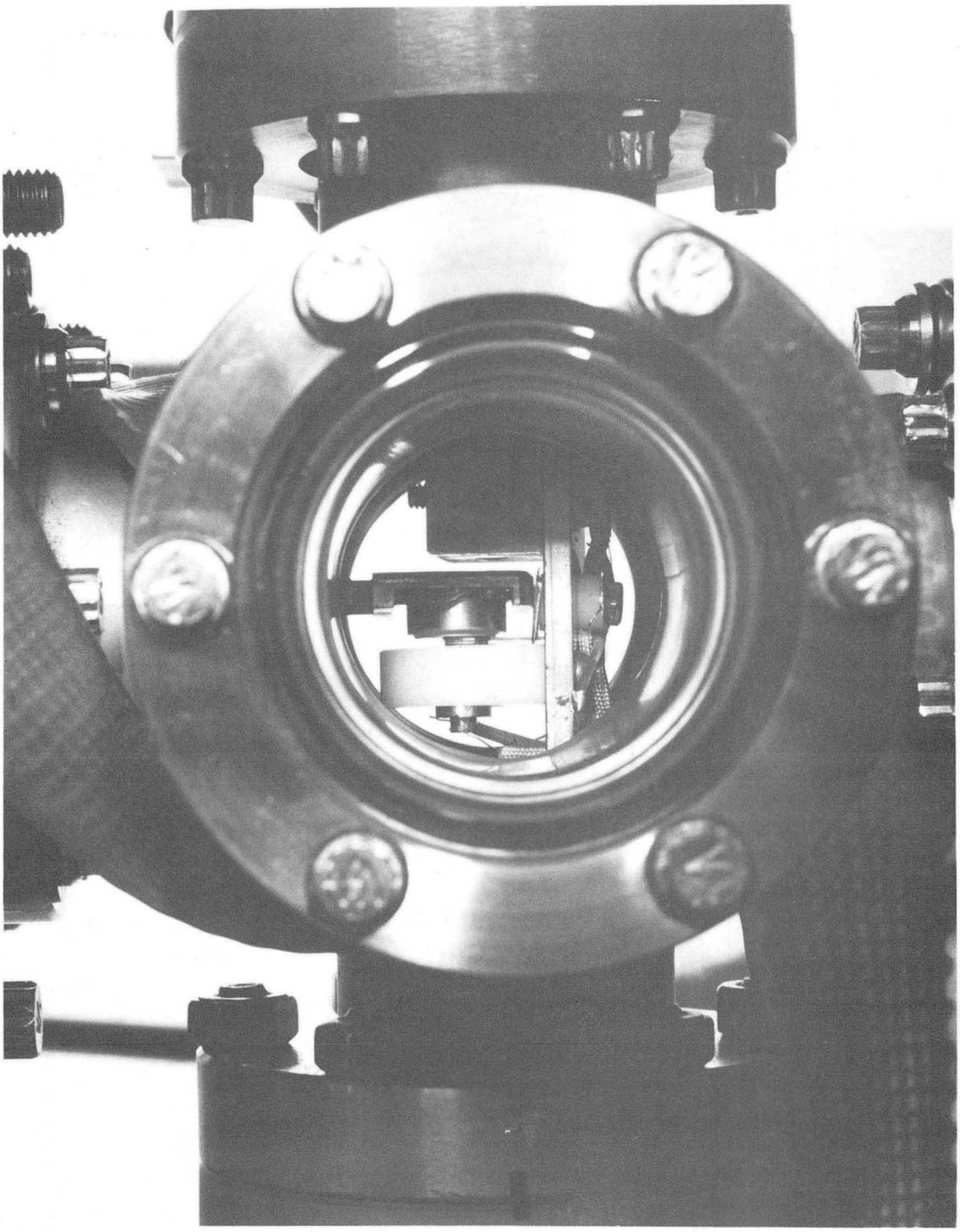

CBB 824-3089

Fig. 2

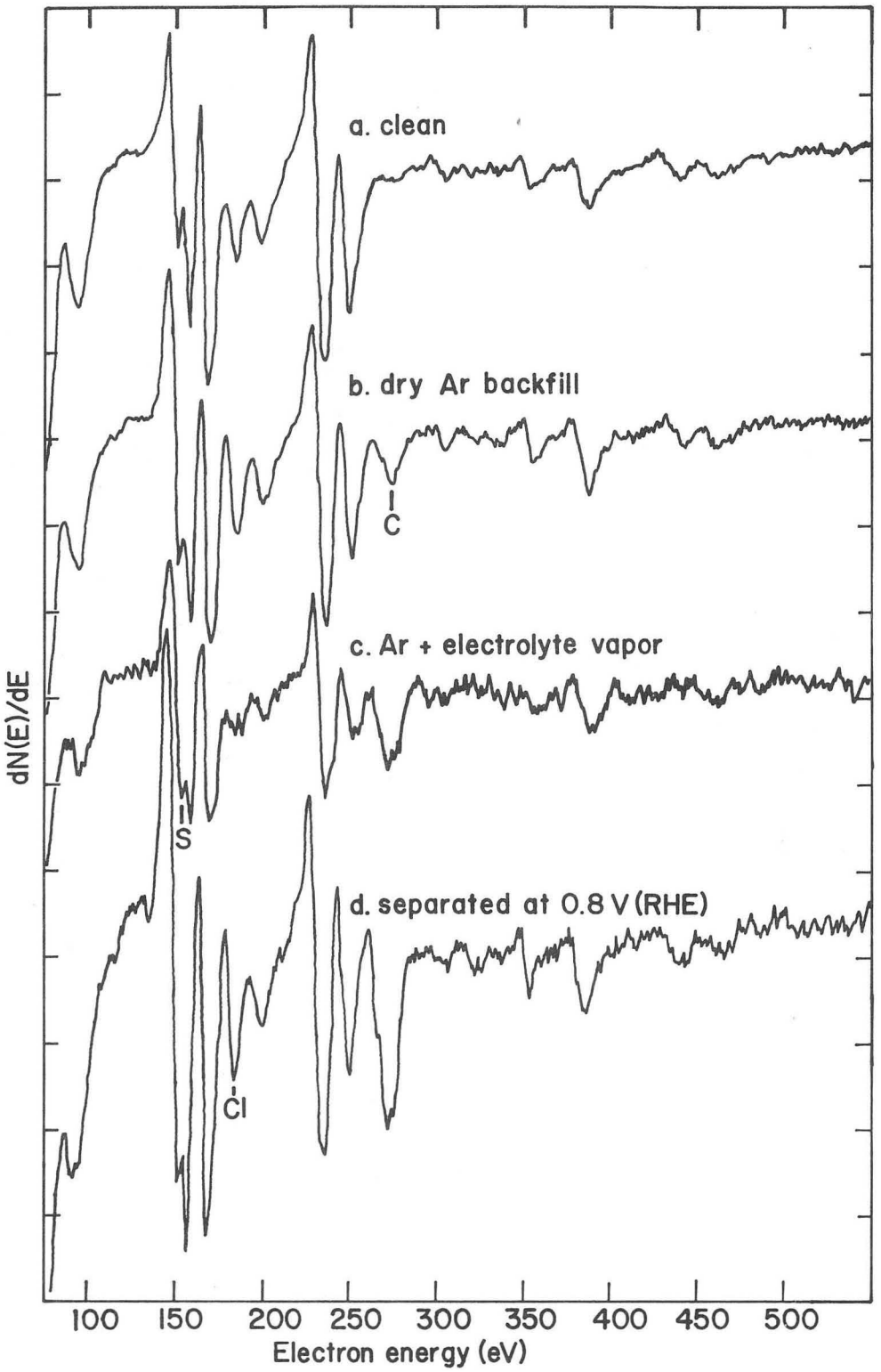
a. clean
b. dry Ar backfill
C
c. Ar + electrolyte vapor
S
d. separated at 0.8 V (RHE)
Cl
dN(E)/dE
100
150
200
250
300
350
400
450
500
Electron energy (eV)
XBL 832-8234

Fig. 3

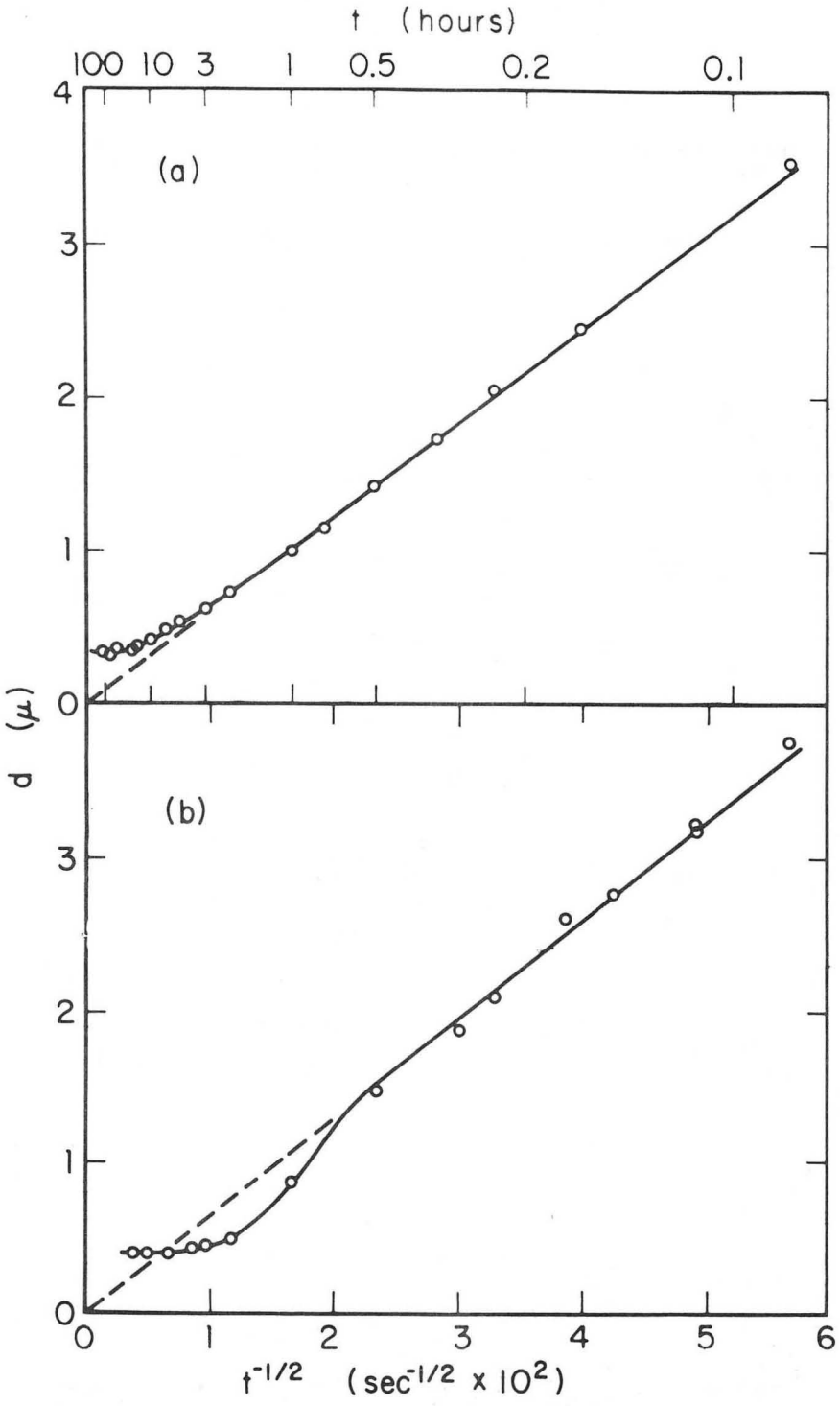
t (hours)
100 10 3 1 0.5 0.2 0.1
(a)
(b)
d (μ)
0 1 2 3 4
0 1 2 3 4 5 6
t^-1/2 (sec^-1/2 x 10^2)
MUB-9185

Fig. 4

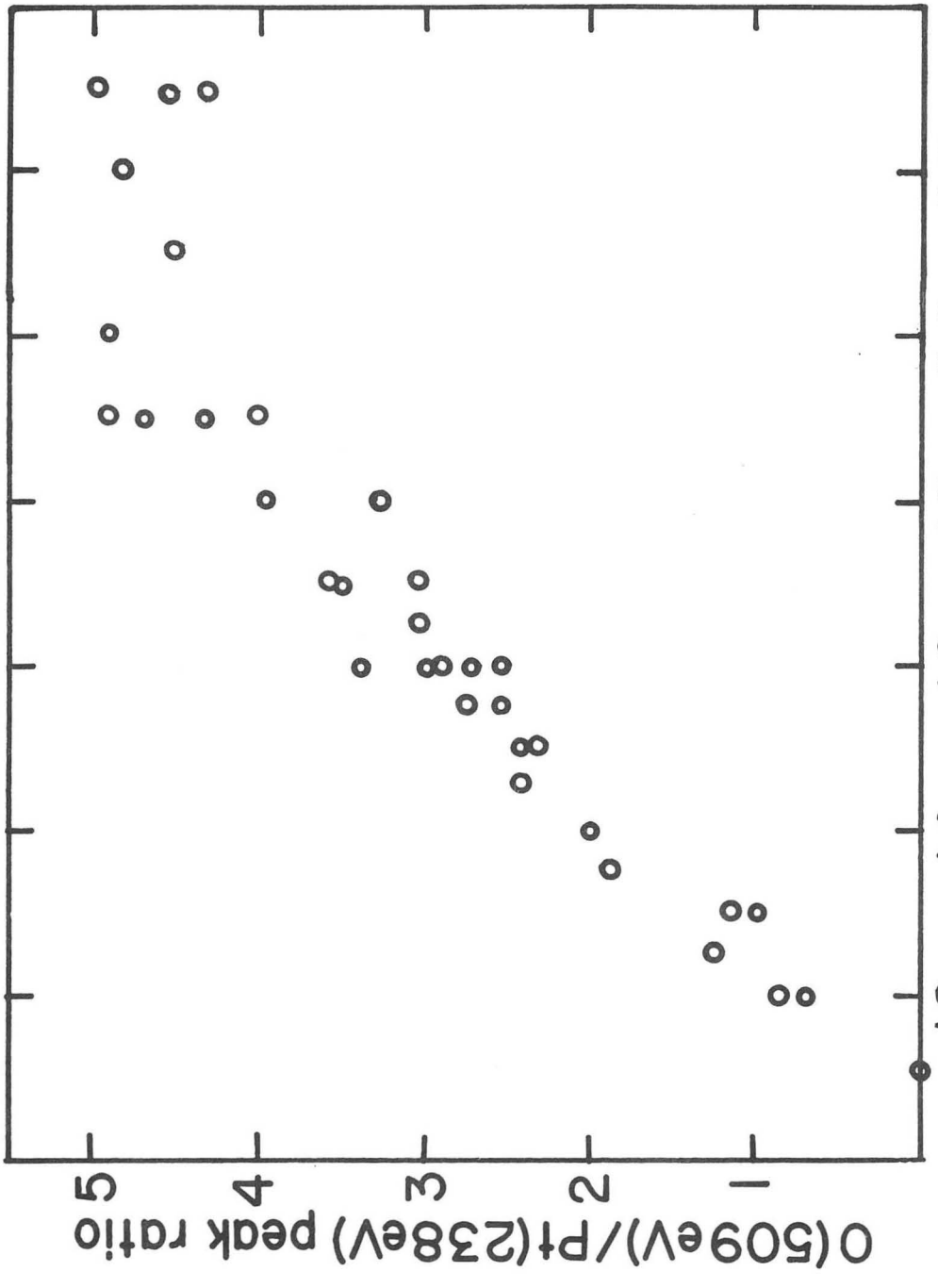

XBL 832-8435

Fig. 5a

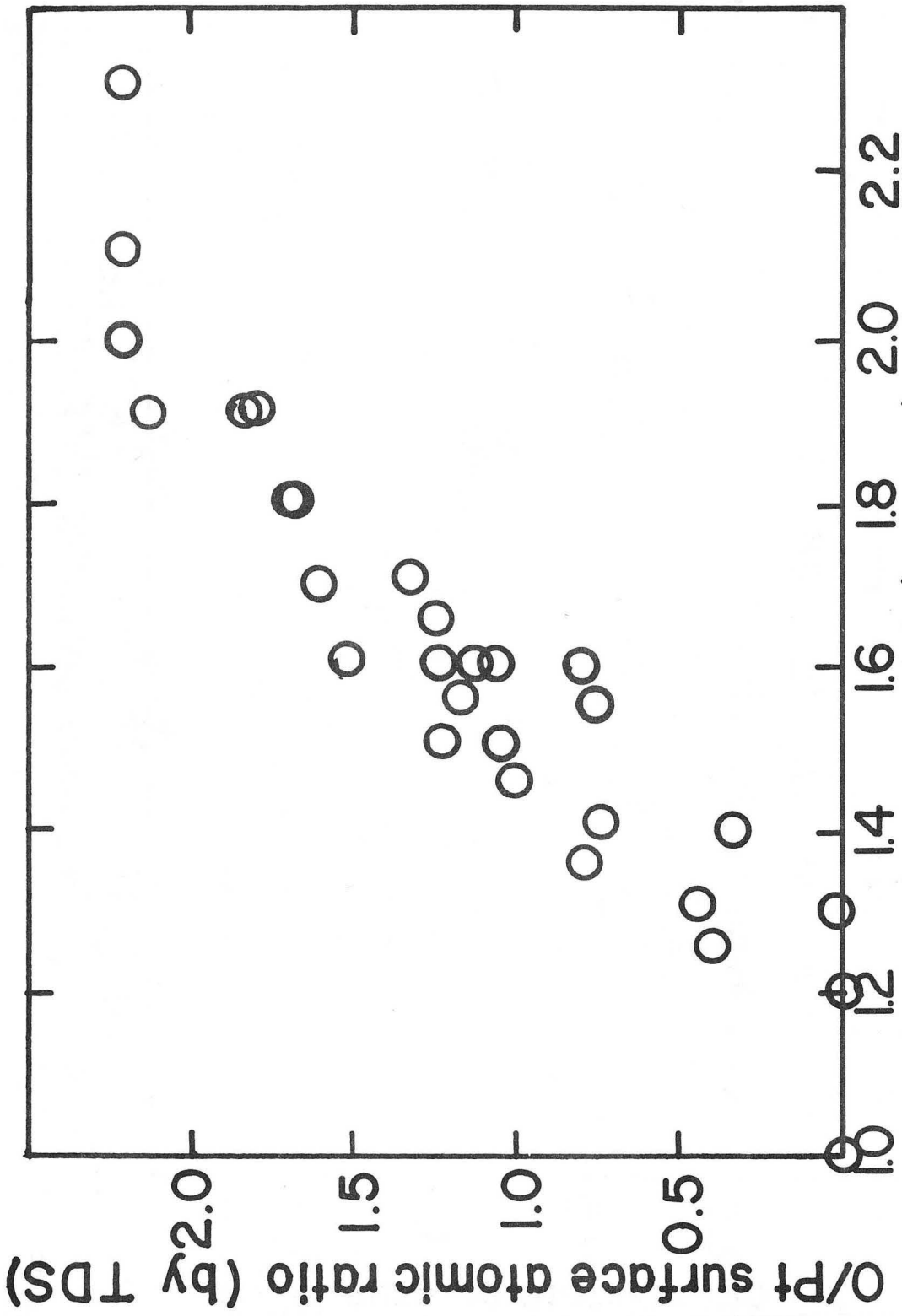

XBL 832-8428

Fig. 5b

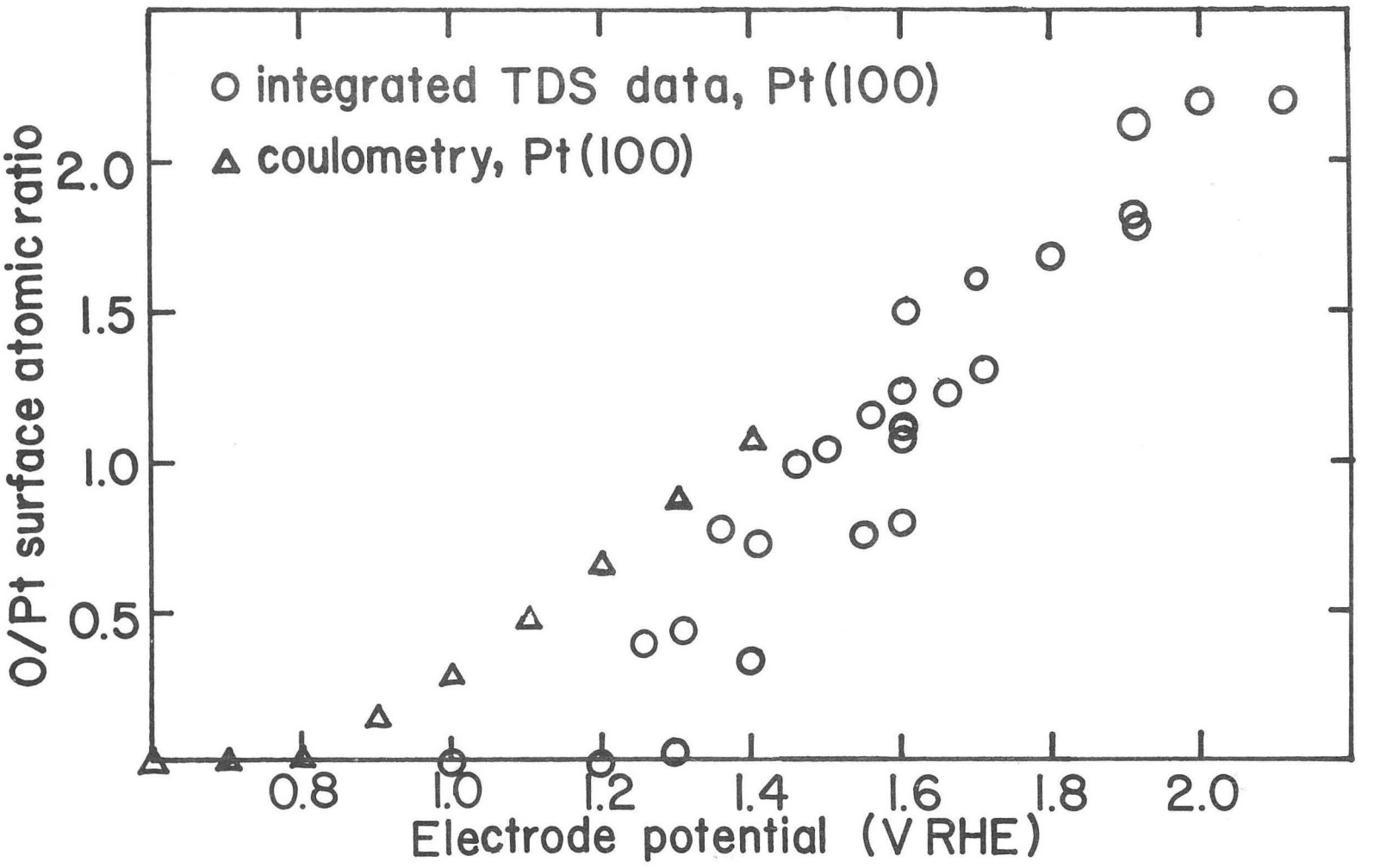

XBL 832-8436

Fig. 6

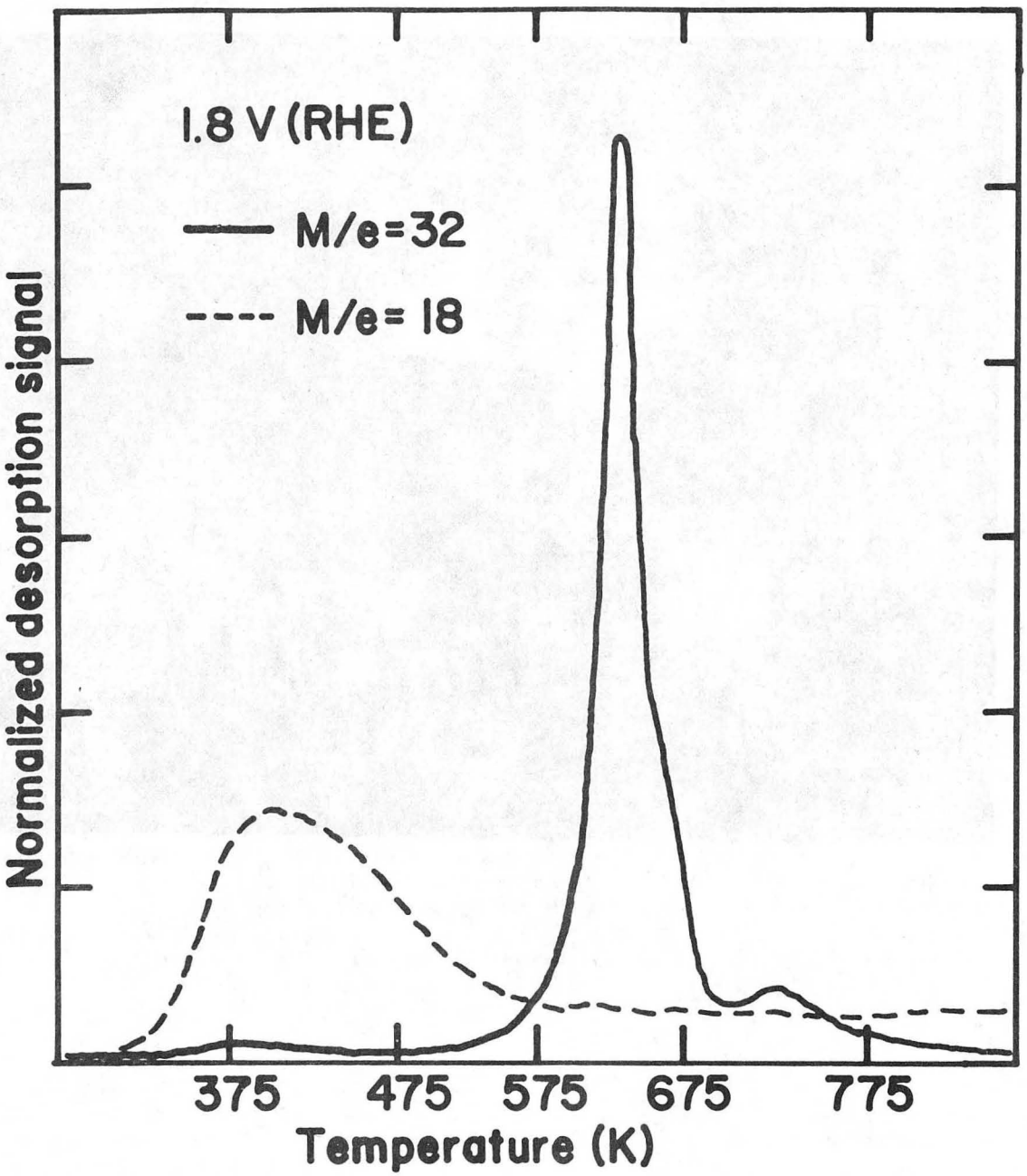

XBL 832-8429

Fig. 7

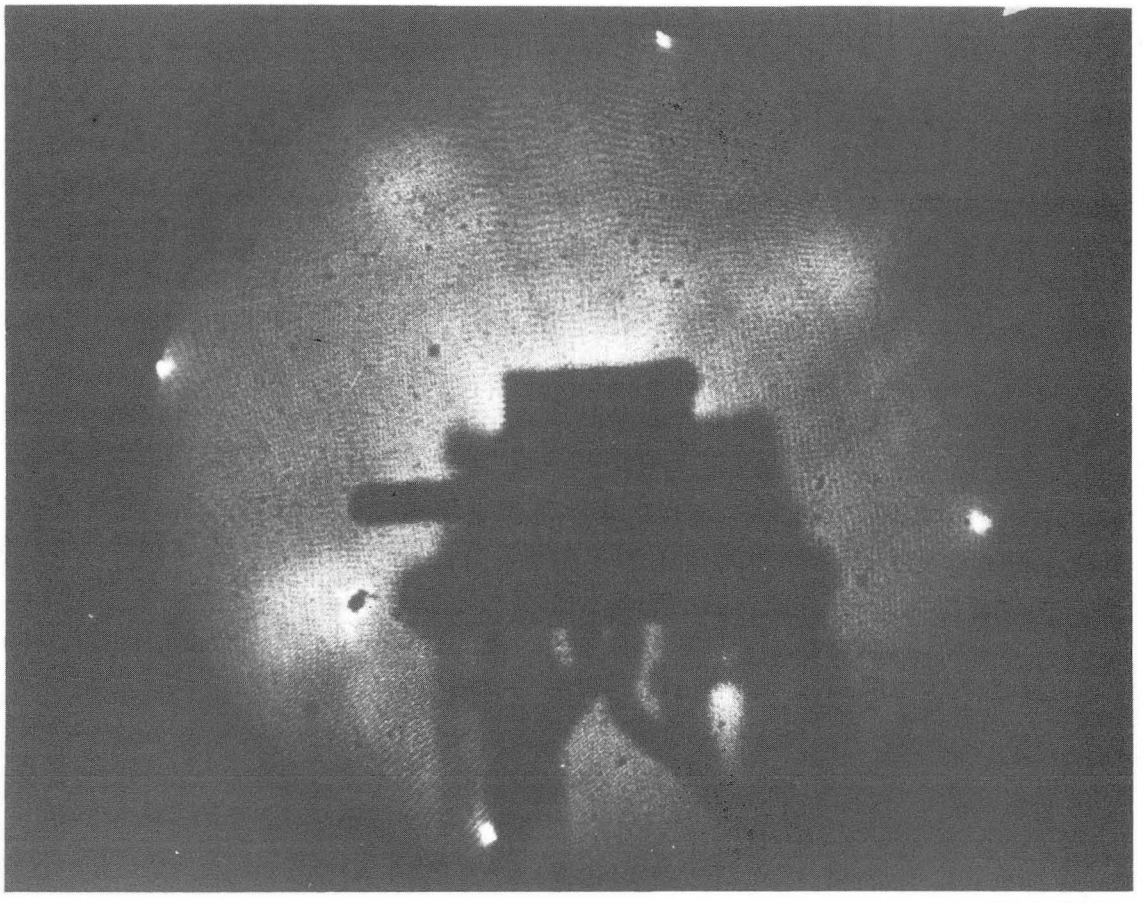

XBB 836-5073

Fig. 8

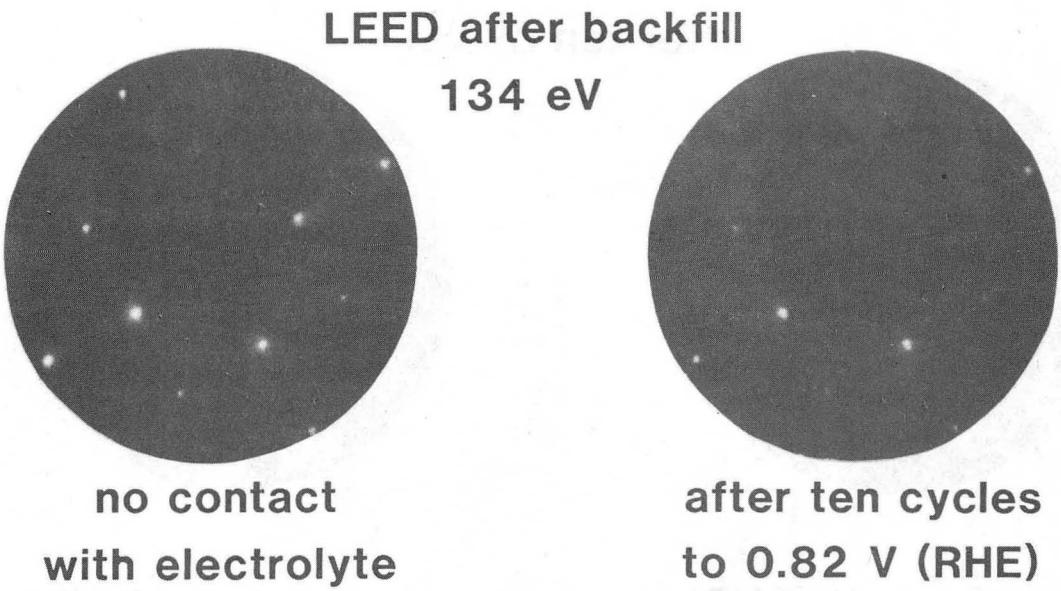

XBB 835-3838

Fig. 9

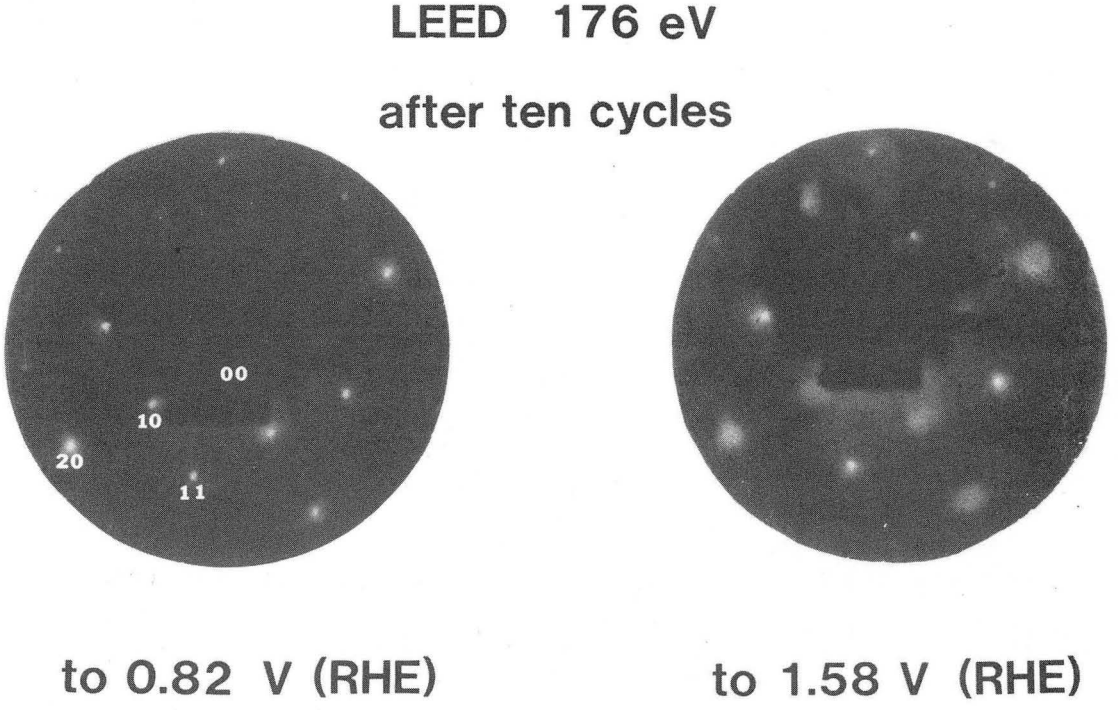

XBB 834-3505

Fig. 10

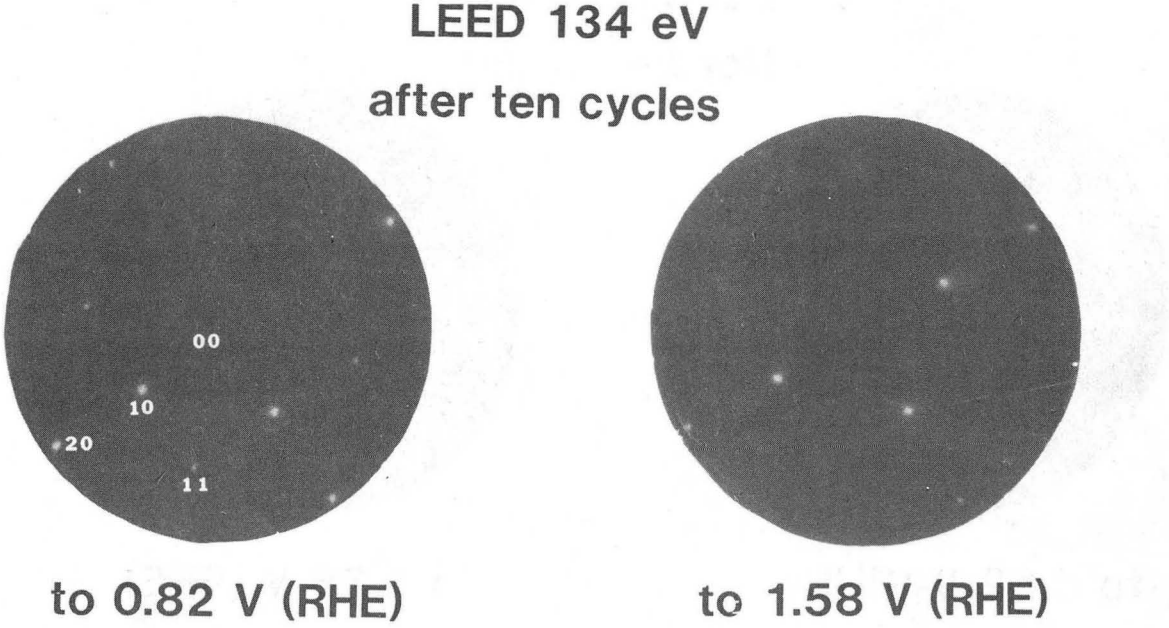

XBB 834-3504

Fig. 11

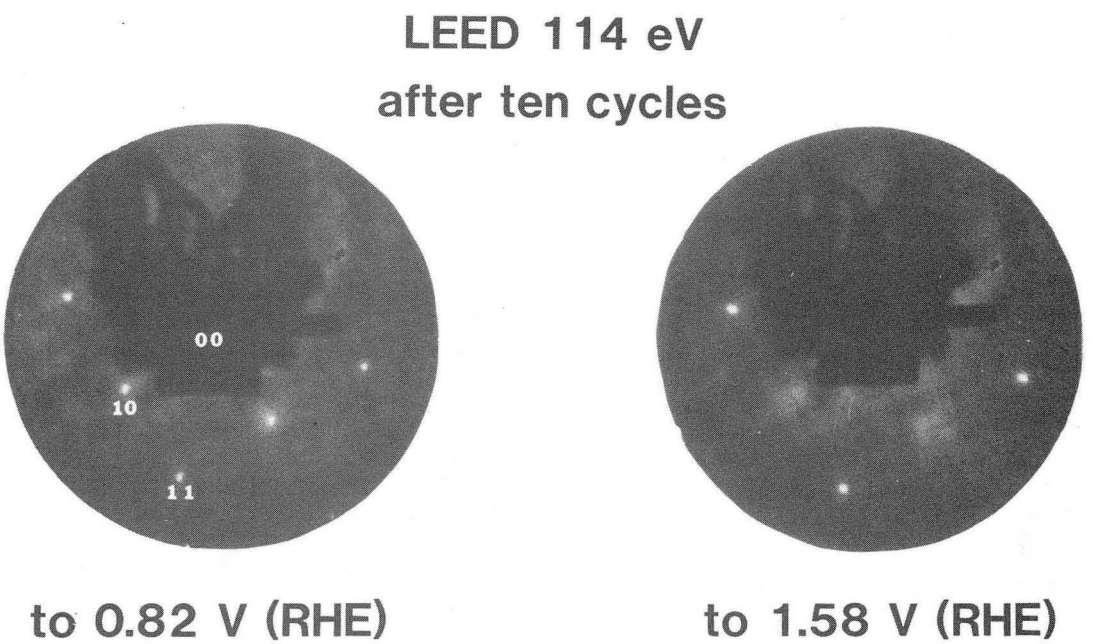

XBB 834-3503

Fig. 12

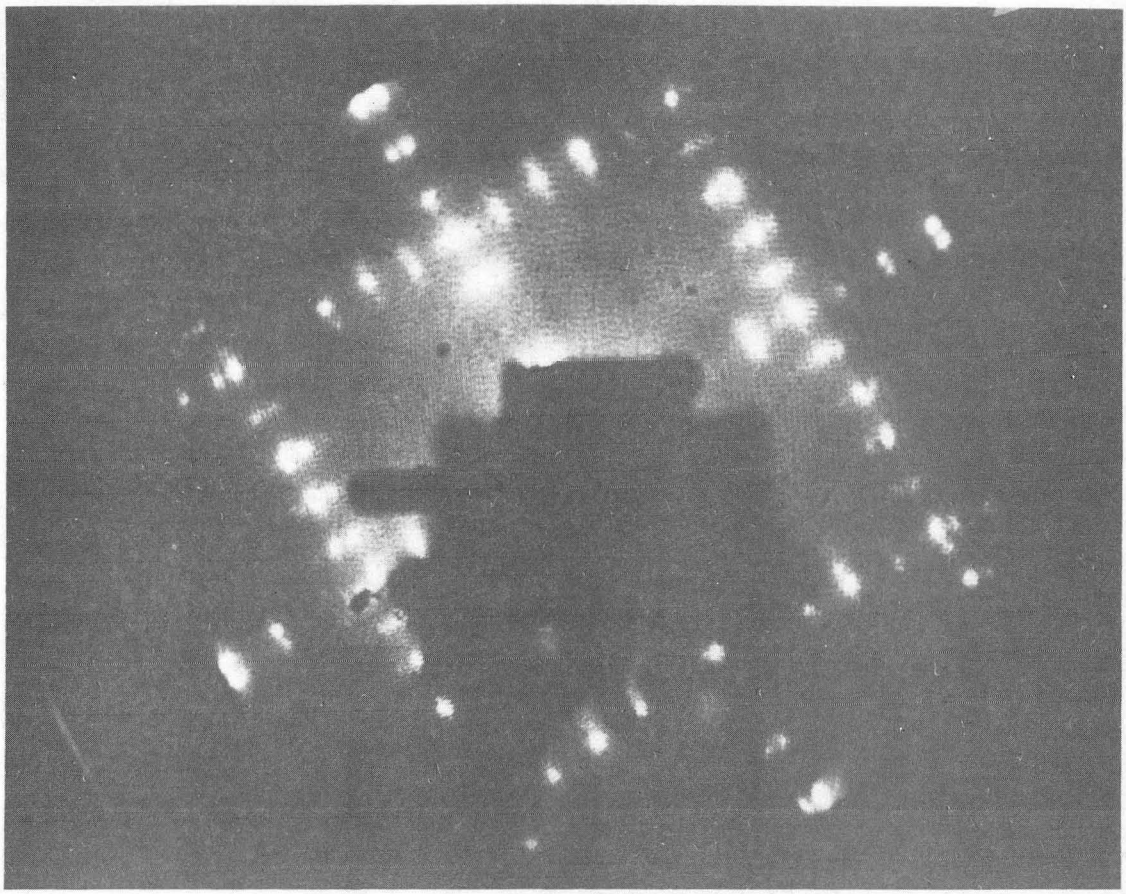

XBB 836-5072

Fig. 13

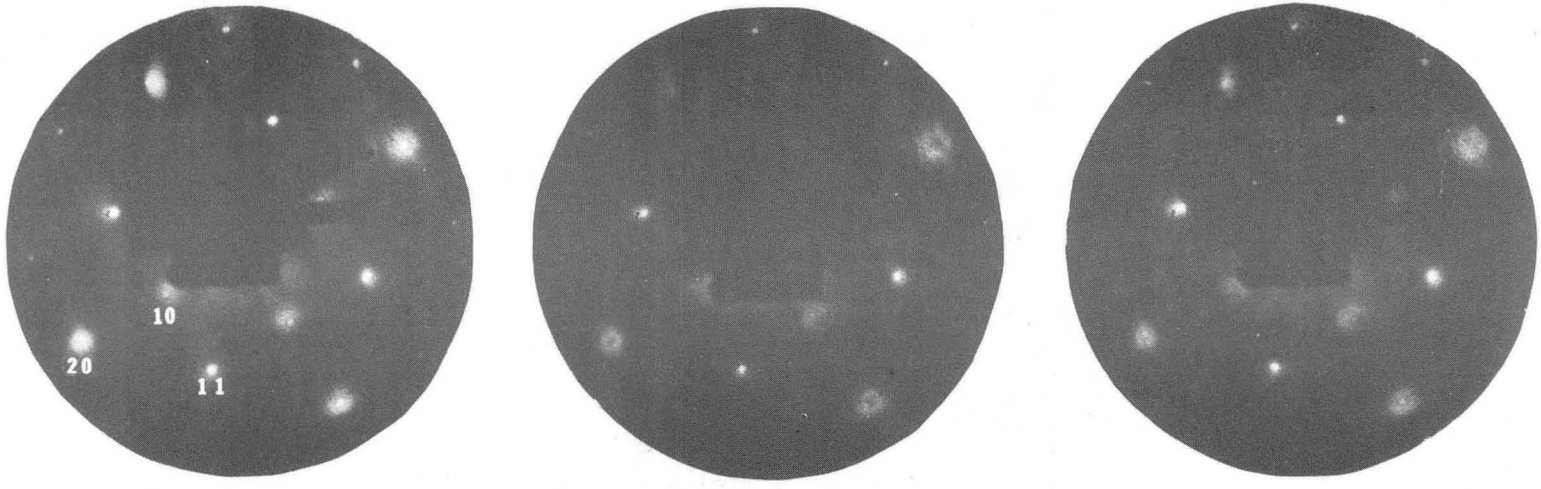

XBB 837-6065

Fig. 14

This report was done with support from the Department of Energy. Any conclusions or opinions expressed in this report represent solely those of the author(s) and not necessarily those of The Regents of the University of California, the Lawrence Berkeley Laboratory or the Department of Energy.

Reference to a company or product name does not imply approval or recommendation of the product by the University of California or the U.S. Department of Energy to the exclusion of others that may be suitable.

TECHNICAL INFORMATION DEPARTMENT
LAWRENCE BERKELEY LABORATORY
UNIVERSITY OF CALIFORNIA
BERKELEY, CALIFORNIA 94720